Université de Montréal

Surface-atmosphere energy exchanges and their effects on surface climate and boundary layer dynamics in the forest-tundra ecotone in northwestern Canada

Par
Vincent Graveline

Département de géographie

Faculté des arts et des sciences

Mémoire présenté en vue de l'obtention du grade

Maîtres ès sciences (M. Sc)

en Géographie

28 avril 2023

Université de Montréal

Département de géographie, Faculté des arts et des sciences

Ce mémoire intitulé

Surface-atmosphere energy exchanges and their effects on surface climate and boundary layer dynamics in the forest-tundra ecotone in northwestern Canada

Présenté par

Vincent Graveline

A été évalué(e) par un jury composé des personnes suivantes

James King
Président-rapporteur

Oliver Sonnentag
Directeur de recherche

Manuel Helbig
Codirecteur

Alexis Maximilien Berg
Membre du jury

Abstract

Considering its vast extent, the Arctic-boreal region (ABR) plays an important role in the global climate system through its exchange of energy and matter with the atmosphere. Air temperature across the ABR has been increasing at a higher rate compared to the global average and has led to changes in vegetation composition and structure across the ABR. The ABR includes the forest-tundra ecotone (FTE), spanning more than 10,000 km across the northern hemisphere. As the world's longest transition zone, the FTE separates the boreal and Arctic biomes over a width of only a few tens to hundreds of kilometers. Vegetation composition and structure varies considerably across the FTE as trees become, from south to north, shorter and more stunted, sparser, and eventually, absent. The associated latitudinal gradient in surface properties results in corresponding latitudinal variations in the energy balance. Thus, changes in the latitudinal variation in surface properties and energy exchanges within the atmospheric boundary layer (ABL) may affect future regional climate across the FTE. The goal of this study was to develop a baseline understanding of the latitudinal variation in surface-atmosphere interactions and atmospheric boundary layer dynamics across the FTE in northwestern Canada. We used paired eddy covariance measurements of surface energy fluxes and supporting environmental measurements at a subarctic woodland ('woodland') and a mineral upland tundra site ('tundra') to quantify differences in daily and seasonal differences in woodland and tundra properties and energy exchanges. Four bulk surface parameters (albedo, aerodynamic conductance, surface conductance, and decoupling factor) were examined to explain drivers of those differences. Campaign-based radiosonde observations and numerical experiments using an ABL model were used to examine the impacts of a sparse tree cover on ABL dynamics (height, temperature, humidity) and their implications for surface climate compared to treeless tundra. The sparse tree cover at the woodland site showed an enhanced ability to transfer heat into the atmosphere and a higher resistance to evapotranspiration compared to tundra, leading to warmer and drier conditions especially in late winter and spring. In summer and fall, higher bulk surface conductance at the tundra site led to more energy being used to moisten the atmosphere, resulting in a shallower ABL and regional cooling of the atmosphere. Refined characterization of land surface-atmosphere interactions across the FTE will help to project the effect of ongoing vegetation changes on regional climate in the circumpolar Arctic-boreal region.

Keywords: Surface energy balance, atmospheric boundary layer, surface properties, forest-tundra ecotone, eddy covariance, mixed-layer slab model, vegetation shifts.

Résumé

La région boréale arctique (RBA) couvre une vaste étendue qui lui confère un rôle important dans le système climatique mondial, par ses échanges d'énergie et de matière avec l'atmosphère. La température de l'air dans la région boréale arctique a augmenté à des taux disproportionnés par rapport à la moyenne mondiale, entraînant des changements dans la composition et la structure de la végétation. La RBA comprend l'écotone de la forêt boréale et de la toundra (EFT), qui s'étend sur plus de 10,000 km à travers l'hémisphère nord. La structure et la composition de la végétation varient considérablement à travers l'EFT. Du sud au nord, les arbres deviennent plus courts, plus dispersés et finalement absents. Ce gradient entraîne des variations dans la balance énergétique de surface. Ainsi, des changements dans la composition et la structure de la végétation dans l'EFT pourraient influencer le climat régional futur de ces régions. Ces changements régionaux pourraient se répercuter sur le climat mondial en interagissant avec le cycle du carbone par des changements dans les régimes de perturbations et la profondeur de la couche limite atmosphérique. L'objectif de cette étude était de développer un état des lieux de la variation latitudinale des interactions entre la surface et l'atmosphère et du climat régional à travers l'EFT dans le nord-ouest du Canada. Nous avons utilisé des mesures de covariance des turbulences provenant d'une forêt subarctique en marge de l'EFT et d'une toundra minérale caractérisant l'EFT du nord-ouest du Canada afin de quantifier les différences journalière et saisonnières des échanges d'énergie. Quatre paramètres de surface (albédo, conductance aérodynamique, conductance de surface et facteur de découplage) ont été examinés dans le but d'expliquer les différences dans la balance énergétique de surface. Des observations par radiosonde basées sur des campagnes de terrain et une expérience de modélisation de la couche limite atmosphérique ont été réalisées afin de discuter des conséquences potentielles des changements de végétation sur la dynamique de la couche limite atmosphérique (hauteur, température, humidité) et ses implications pour le climat régional. La forêt subarctique a démontré une meilleure capacité à transférer la chaleur vers l'atmosphère et une plus grande résistance à l'évapotranspiration, se traduisant par des conditions atmosphériques plus chaudes et sèches, spécialement au printemps. En été et automne, une conductance de surface plus élevée sur le site de la toundra s'est traduite par à une plus grande proportion de l'énergie utilisée pour humidifier l'atmosphère, résultant en une couche atmosphérique moins épaisse et un refroidissement régional du climat. La caractérisation des interactions entre la surface et

l’atmosphère à travers l’EFT contribuera à améliorer les prédictions des effets des changements de végétation en cours sur le climat régional dans la région boréale arctique.

Mots-clés : Balance énergétique de surface, couche limite atmosphérique, propriétés de surface, écotone forêt-toundra, covariance des turbulences, modélisation de la couche limite atmosphérique.

Table of contents

List of figures

Glossary

FTE	Forest-tundra ecotone
ABL	Atmospheric boundary layer
ABR	Arctic-boreal regions
H	Sensible heat flux
LE	Latent heat flux
Rn	Net radiation
G	Ground heat flux
SWin	Incoming shortwave radiation
SWout	Outgoing shortwave radiation
LWin	Incoming longwave radiation
LWout	Outgoing longwave radiation
Ga	Aerodynamic conductance
Gs	Surface conductance
Ω	Decoupling factor
α	Albedo
VPD	Vapour pressure deficit
HPC	Havikpak Creek
TVC	Trail Valley Creek
LAI	leaf area index

MAAT	Mean annual air temperature
MATP	Mean annual total precipitation
MSAT	Mean summer air temperature
MSTP	Mean summer total precipitation
MWAT	Mean winter air temperature
MWTP	Mean winter total precipitation
°C	Degree Celsius
θ	Potential temperature
q	Specific humidity
Δθ	Diurnal change in potential temperature within the atmospheric boundary layer
Δq	Diurnal change in specific humidity within the atmospheric boundary layer
CLASS	Chemistry Land-surface Atmosphere Soil Slab model
EF	Evaporative fraction
R2	Coefficient of determination

Acknowledgments

I would like to start by thanking the Inuvialuit community of Inuvik and the Aurora Research Institute granting permission to conduct my research in their homeland. Spending time in Inuvik was a unique experience for me and I will remember it for the rest of my life. I am deeply thankful and salute the work, the implication, the support, the accessibility and the patience of both my directors, Oliver Sonnentag and Manuel Helbig. You made my master thesis a unique and enriching experience and I really enjoyed working with you. I would like to thank you both for pushing me toward different opportunities that made me grow as a scientist but also as a person, such as the opportunity to discover the Arctic, my stay in Halifax, my internship at Ouranos, and the chance to present my work by attending several workshops and conferences. I feel lucky to have had the chance to work with you and I will certainly keep good memories of these years. I would also like to thank the several members of the Laboratory in Atmospheric Biogeosciences in High Latitudes (Atmosbios) for the good moments, the laughs and their support. I would like to especially thank Gabriel Hould Gosselin and Charles Gauthier for their help and the good moments in the field. Finally, I am grateful for the support and the encouragement of my family, my friends and my girlfriend, especially toward the end of my master thesis.

Chapter 1

Context and research objectives

This first chapter presents a literature review of land surface-atmosphere interactions at the forest-tundra ecotone (FTE), outlining how vegetation composition and structure across the FTE might change as a result of climate warming. Next, the complex interaction between the land surface, the surface energy balance, and the role of the atmospheric boundary layer (ABL) on surface climatic conditions are discussed. The challenging conditions and relative inaccessibility of Arctic-boreal regions make them challenging areas to study. This literature review presents existing knowledge on land surface-atmosphere interactions at the FTE and provides context for the main research objectives of this study.

1.1 Vegetation shifts in the forest-tundra ecotone

The Arctic-boreal region (ABR) plays an important role in the global climate through its exchange of energy and matter with the atmosphere (McGuire et al., 2006). It has been warming much faster than the global average (Rantanen et al., 2022). Ecosystems of the ABR are experiencing changes in their vegetation structure and composition in response to this warming. Climate warming leads to various consequences, such as changes in precipitation patterns (Hinzman et al., 2005), disturbance regimes (Foster et al., 2022) and permafrost thawing (Helbig et al., 2016). As a result, changes in the vegetation structure and composition have been observed across the ABR (Berner & Goetz, 2022; Harsch et al., 2009; Rees et al., 2020).

The FTE acts as a transition zone between the coniferous boreal forest characterized by varying degrees of tree coverage and the treeless arctic tundra, spanning more than 10,000 km across the northern hemisphere (Callaghan et al., 2002), with around 4,800 km in North America (Lafleur & Rouse, 1995). The structure of the FTE is characterized by a gradient in vegetation structure and composition from south to north, where trees dominating in the southern margin of the FTE, gradually decrease in height and become sparse, and eventually vanish, giving way to a treeless tundra landscape. The latter is characterized by medium and low shrubs, lichens, and tussocks, sedge meadows, and peat ice wedge polygons (Timoney et al., 1992). Tree growth forms

dominate the understory species south of the FTE whereas dwarf shrubs and graminoids dominate at the northern edge (Callaghan et al., 2002).

The FTE, often referred to as treeline, is expected to undergo changes with rising temperature. Most likely, trees and shrubs could establish further north in a warming climate as predicted by dynamic global vegetation models (Pearson et al., 2013; Zhang et al., 2013) and seen in the late 1800s at the end of the ‘’Little Ice Age’’ (Holtmeier & Broll, 2007).

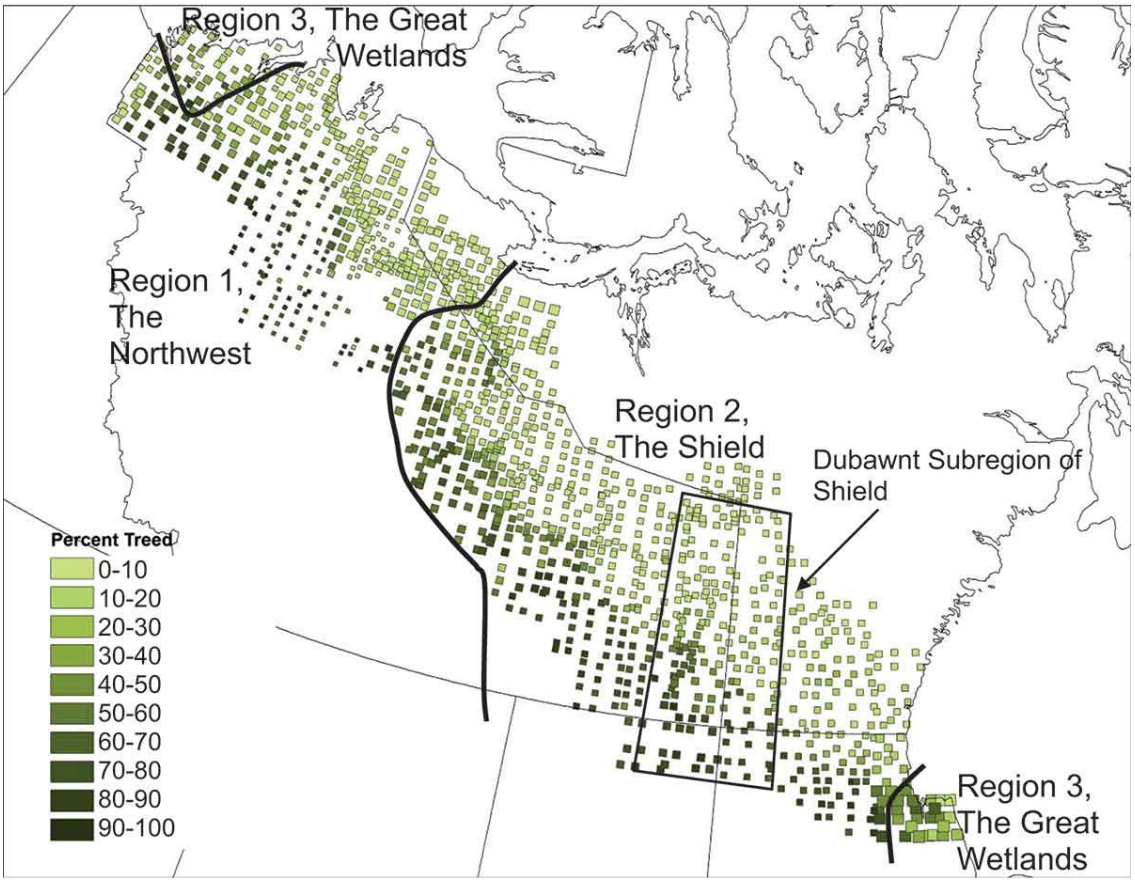

FIGURE 1.1 - Present tree cover at the FTE as estimated in Timoney and Mamet (2020). Forest tree cover was estimated from 1314 air photo footprints and overlaying of the Global Forest Change (GFC) tree cover data (green color shading).

Some studies support the hypothesis that biome shifts of the FTE into the tundra have occurred over the 20th century around the circumpolar north (Berner & Goetz, 2022; Harsch et al., 2009; Rees et al., 2020). However, evidence of recent northward shifts of boreal and subarctic ecoregions is still debated (Timoney, 2022). Timoney and Mamet (2020) have observed modest to nonsignificant afforestation in northwestern Canada and no significant evidence of northward

migration of trees across subarctic central and western Canada since 1960. Lantz et al. (2019) discovered a significant increase in the stand density of white spruce (*Picea glauca* (Moench) Voss) since 1980 in 52 locations across the FTE in Northwest Territories, Canada, but not in the tundra. Similarly, Travers-Smith and Lantz (2020) observed an increase in alder and spruce stem density in the Tuktoyaktuk Coastal Plain, NWT, from 1970 to 2000, without any changes to their range limits. Slight differences in geography are sufficient to produce large differences in tree growth climate responses (Lloyd et al., 2002). In the Inuvialuit Settlement Region of northwestern Canada, shrub cover has been expanding within the low Arctic tundra, extensively in the boreal forest-tundra transitional zone, by on average 4.2% per decade (Nill et al., 2022).

Changing disturbance regimes are also believed to play an important role in biome shifts in the ABR. Boreal Forest conversion to woodlands, shrublands, or grasslands has been documented after recent wildfires, particularly in warm and dry regions of the FTE (Baltzer et al., 2021; Kukavskaya et al., 2016). On the other hand, wildfires can facilitate forest expansion into Arctic tundra by improving seedbed conditions (Lloyd & Bunn, 2007). Wildfire activity is expected to increase with rising temperatures (Walker et al., 2020) and will contribute to vegetation shifts at the southern and northern margins of the boreal forest (Gonzalez et al., 2010; Stralberg et al., 2018). Vegetation shifts at the FTE result from complex ecological and climatological processes. However, the FTE is undoubtedly experiencing change in the composition and structure of its vegetation and better understanding how such shifts could affect the regional climate has the potential to improve future climate predictions. Other studies have shown a cooling and moistening effect of boreal forest loss on regional climate due to post-fire changes to the energy balance (Ueyama et al., 2020) and due to permafrost thaw-induced boreal forest loss (Helbig et al., 2016) increasing LE at the expense of H. Thus, changes in the latitudinal variation in surface properties and energy exchanges with the ABL may affect future regional climate across the FTE.

1.2 Surface energy balance

Land use change impacts on climate are commonly quantified by determining the energy used to directly warm or moisten the atmosphere and how it affects net radiation at the surface via albedo changes (Baldocchi & Ma, 2013; Beringer et al., 2005; Chapin et al., 2005; Eaton et al., 2001; Eugster et al., 2000; Helbig. et al., 2016; Lafleur & Rouse, 1995). The gradient in land surface properties at the FTE results in variations in energy exchanges with the atmosphere that affect

regional climate (Beringer et al., 2005; Eugster et al., 2000). Surface properties modulate, among other things, the reflection of solar radiation (albedo) and the transfer of heat and humidity between the surface and the atmosphere, thus its partitioning into sensible heat flux (H) and latent heat flux (LE).

Surface properties affect the surface energy balance by controlling the available energy (**Fig. 1.2**). Net radiation (Rn, net radiation) represents the balance between incoming and outgoing shortwave and longwave radiation (**Eq.1**). Shortwave radiation is emitted by the sun and provides energy to the Earth system. Some of this radiation is absorbed or reflected by the atmosphere and the Earth's surface (albedo, i.e., fraction of solar radiation that is reflected). Part of the energy absorbed by the surface is reemitted as longwave radiation. The energy that remains contributes to warming of the soil as a ground heat flux (G), to warm the air, or to moisten the air (**Eq.2**) (Trenberth et al., 2009). Sensible heat (H) warms the air above the surface and is transported into the atmosphere by turbulent motion while latent heat (LE) is stored in water vapour and is associated with evapotranspiration (Beringer et al., 2005).

(**Eq.1**) Rn = SWin - SWout + LWin – LWout

(**Eq.2**) $LE + H = Rn - G$

Surface properties can be characterized by bulk surface parameters. Commonly used, the bulk aerodynamic conductance (Ga) (m s^{-1}) (Thom, 1972) expresses the capacity of the surface to generate momentum or turbulence, responsible for the transport of water vapour and heat into the atmosphere. Bulk surface conductance (Gs) (m s^{-1}) (Monteith., 1965) additionally describes the efficiency of water vapour transport through leaf stomata and surface soils into the atmosphere. The decoupling factor (**Ω**) indicates the degree of coupling between the land surface and the atmosphere, ranging from 0, when evapotranspiration is controlled by Gs and vapour pressure deficit, to 1 when evapotranspiration is controlled by Rn (McNaughton & Spriggs, 1986; Ryu et al., 2008). Albedo determines the fraction of absorbed shortwave incoming radiation and partly controls available energy to be partitioned into H and LE. Bulk surface parameters can be derived from turbulent flux and radiation measurements.

Boreal and arctic ecosystems do not allocate the same proportion of the energy received to evapotranspiration and to sensible heating. Beringer et al. (2001) demonstrated how surface

properties shape these fluxes in their study in Alaska over a single growing season. In addition to transmitting more energy to the atmosphere as a result of a lower albedo compared to the tundra, the forest ecosystems use available energy largely in the form of sensible heat, leading to higher air temperatures. Tundra emits a greater proportion of energy as latent heat, resulting from abundant moisture in mosses and no stomatal control over water loss (Beringer et al., 2005). Lafleur and Rouse (1995) examined the interannual variability in energy fluxes of a boreal forest and a wetland tundra site at the FTE in the Hudson Bay Lowlands during the summers of 1989 - 1993. Similarly, they found that summer H was larger and LE smaller over the boreal forest stand than over the wetland tundra. The heterogeneity of northern ecosystems leads to variations in surface properties from one region to another and thus regional climate responses might also differ (Denissen et al., 2021).

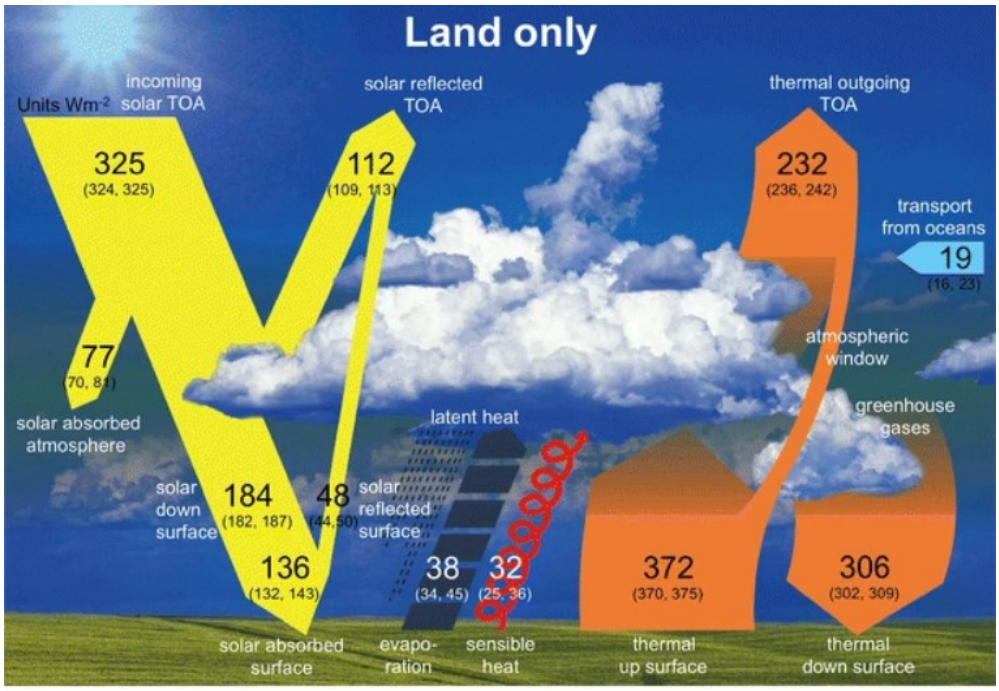

FIGURE 1.2 - Best estimates for the magnitude of the annual mean energy balance components averaged over land (upper panel) and oceans (lower panel), together with their uncertainty ranges, representing climatic conditions at the beginning of the twenty-first century. The surface thermal upward flux contains both the surface thermal emission and a small contribution from the reflected part of the downward thermal radiation. Units Wm−2 (Wild et al., 2014).

In the FTE, a decrease in albedo is generally found across the gradient from the boreal forest to the arctic tundra (Beringer et al., 2005). The presence of trees creates a darker and rougher (more irregular) surface than tundra vegetation. The effect of albedo is particularly striking when snow is covering the ground. This large difference in albedo during snow season results in greater differences in energy partitioning (Thompson et al., 2004). The amount of energy absorbed by the forest canopy is larger, thus more energy is available to be emitted to the atmosphere in the forest. Moreover, LE is necessarily smaller in winter, since water is often still frozen in the ground and unavailable for the vegetation (Beringer et al., 2001).

The explicit determination of the partitioning of H and LE fluxes is what makes it possible to link the evolution of air temperature and humidity to surface properties (Vila-Guerau de Arellano et al., 2015). Surface heat fluxes can be continuously observed with the eddy covariance (EC) technique (Baldocchi, 2003) alongside measurements of radiative fluxes and ground heat fluxes. The EC technique allows direct measurement of H and LE fluxes at the ecosystem scale. Flux footprints can extend from hundreds of meters to several kilometers and are measured continuously over long periods (Baldocchi, 2003). The EC technique relies on the use of micrometeorology theory to interpret the high-frequency covariance of vertical wind speeds and scalar concentrations in the atmosphere (Baldocchi, 2003). Quasi continuous flux estimates at half-hourly time steps covering entire weeks, months and years are provided. This technique is now widely used to assess land surface-atmosphere interactions (Baldocchi & Ma, 2013; Beringer et al., 2005; Helbig et al., 2020; Helbig. et al., 2016; Ueyama et al., 2020) and multiple EC systems have been deployed across the Arctic-Boreal region.

1.3 Atmospheric boundary layer dynamics and its implications for surface climatic conditions

The ABL can be defined as the troposphere layer that is directly influenced by the land surface and its forcings (Stull 1988). It generally extends between 1 and 3 kilometers above the surface during the day and is subject to a diurnal cycle (**Fig. 1.3**). The ABL grows during daytime because of buoyancy generated by surface inputs of sensible heat and the entrainment of dry air from the free atmosphere. Surface climatic conditions are therefore closely linked to the ABL, and its evolution

depends largely on the partitioning of available energy into H and LE at the surface (Vila-Guerau de Arellano et al., 2015).

The forcing of the surface onto the lower atmosphere occurs through the transfer of momentum and quantities such as moisture, heat, pollutants and other by turbulence (Vila-Guerau de Arellano et al., 2015). Turbulence can originate from wind shear at the surface, generally referred to as dynamic or mechanical turbulence. However, thermal turbulence associated with H, is mainly responsible for the development of high ABLs. Thermal turbulence results from the warming of the surface, leading to a decrease in air density above the surface compared to the colder air above, creating thermal convection. The rise of warmer air parcels in altitude results from a positive vertical pressure gradient force. Warmer, less dense air rises as eddies and helps to homogenize the properties of the ABL such as pollutants concentration, humidity, and air temperature. This homogenized layer is referred to as the mixed-layer or convective layer (**Fig. 1.3**). The warming of the surface begins as the sun rises, the ABL starts to grow while exchanges of heat and water vapour occur between the surface, the mixed-layer and the free atmosphere (**Fig. 1.3**). Strong winds and rough surface cause greater dynamic turbulence (Stull, 1988; Thompson et al., 2004) and contributes to amplify vertical thermal turbulence and thus to promote moisture and heat fluxes and their mixing in the atmosphere (Vila-Guerau de Arellano et al., 2015). Eddies sometimes reach the upper limit of the ABL characterized by a temperature inversion. Entrainment of dry and warm air in the ABL from the free atmosphere, which is not subjected to surface forcing, occurs when eddies penetrate this capping inversion (**Fig. 1.3**) referred to as the entertainment zone (Vila-Guerau de Arellano et al., 2004). This results in the addition of sensible heat to the mixed layer. It is through this process that the ABL extends into the atmosphere, dragging more and more air from the atmospheric layer above itself (Stull, 1988).

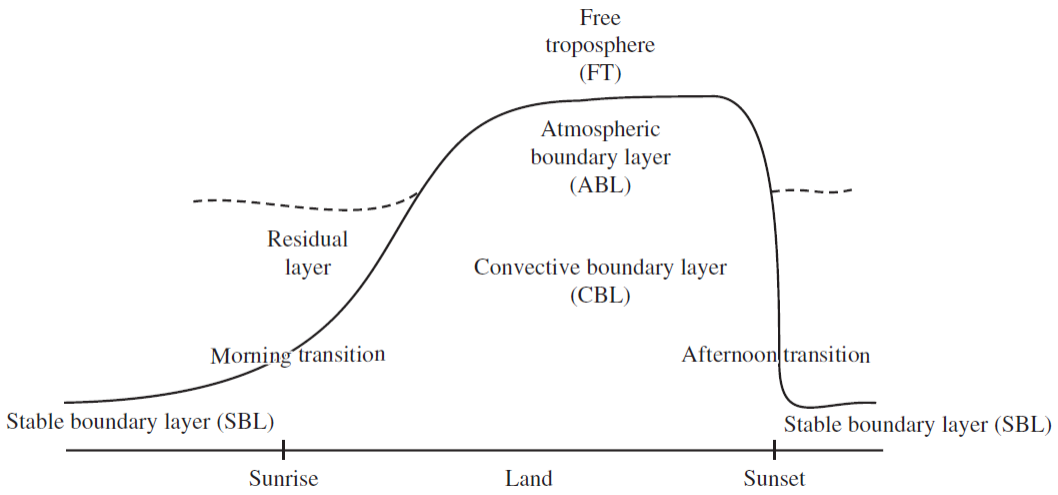

FIGURE 1.3 - Schematic representation of the temporal evolution of the atmospheric boundary layer and the relevant regions that determine its structure and characteristics (Vila-Guerau de Arellano et al., 2015).

Atmospheric boundary layer growth dynamics are often analysed in the context of regional climate feedbacks (Baldocchi et al., 2000; Baldocchi & Ma, 2013; Helbig. et al., 2016; Ueyama et al., 2020). Atmospheric boundary layer height can be defined as the top of the mixed layer (Ueyama et al., 2020) or the middle of the entrainment layer (Rey-Sanchez et al., 2021).

Evaporation of the surface helps to reduce the warming of the air and thus to reduce the growth of the ABL while moistening it (van Heerwaarden et al., 2009). Surface fluxes, by changing the air temperature and moisture content of the ABL also change its evaporative water demand (van Heerwaarden et al., 2009). Two factors control the humidity content of the ABL in the absence of external advection, the evapotranspiration from the surface and the entrainment of dry air at the top of the ABL. The entrainment process leads to reduced specific humidity in the ABL (**Fig. 1.4**). Entrainment of dry air therefore influences the vapour pressure deficit (VPD) of the atmosphere. Indeed, a higher ABL leads to more diluted quantities inside it. The heat capacity will also increase, requiring more heat to increase temperature (Stull, 1988). The entrainment of dry air increases the VPD in the lower atmosphere, but the opposite is also true, wetter conditions in the free atmosphere can lead to a decrease in water demand by bringing moist air into the ABL and thus modulate surface heat fluxes partitioning. Although, this is rather unusual (Vila-Guerau de Arellano et al., 2015).

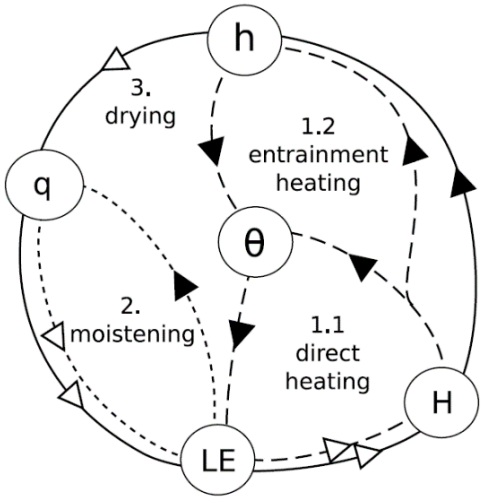

FIGURE 1.4 - Feedback in the coupled land–atmosphere system. Closed arrows represent positive relationships, and open arrows negative relationships. Each of the three feedback has a distinct line style. LE is the latent heat flux, H is the sensible heat flux, θ is potential temperature of the ABL (temperature that an air parcel would attain if adiabatically brought to a standard reference pressure), q is the specific humidity of the ABL, and h is the ABL height (van Heerwaarden et al., 2009).

Interactions between surface fluxes and ABL dynamics can be assessed using mixed-layer slab models that simulate the development of the ABL (McNaughton & Spriggs, 1986). Such models have been used to assess land use change impacts on land surface-atmosphere interactions (Baldocchi & Ma, 2013; Helbig et al., 2016; Rey-Sanchez et al., 2021; Ueyama et al., 2020). Mixed-layer slab models are based on mixed-layer theory in which all quantities such as water vapour, pollutant and heat are vertically well mixed within the ABL (McNaughton & Spriggs, 1986). Changes of any quantity within the mixed-layer result from surface H and LE fluxes and from the entrainment of air from the free troposphere into the ABL (Vila-Guerau de Arellano et al., 2015).

1.4 Goal and objectives

Interest in the FTE has mainly focused on its spatial characterization and future potential vegetation shifts. These are complex and will vary from one region to another. Arctic-boreal regions are hard to study due to their remoteness and harsh environmental conditions. Thus, very few studies were able to compare regional climate and land-atmosphere energy exchange at the FTE under similar

climate conditions over an extended period of time. Even fewer studies were able to link surface properties to ABL dynamics and its implications for surface climatic conditions.

The goal of this study was to develop a baseline understanding of the latitudinal variation in surface-atmosphere interactions and atmospheric boundary layer conditions across the FTE in northwestern Canada. This goal is achieved using close to 10 years of quasi-continuous paired EC measurements from two sites characteristic of the FTE, and a mixed-layer slab model. This study was possible due to the close proximity of the tower sites and the radiosonde observatory, controlling for potential differences in large-scale climate conditions when analyzing differences in surface fluxes and ABL dynamics. Bulk surface parameters are used to explain differences in surface fluxes partitioning and the latter are used to run the mixed-layer slab to quantify ABL growth impact on air temperature and humidity.

Chapter 2

Surface-atmosphere energy exchanges and their effects on surface climate and boundary layer dynamics in the forest-tundra ecotone in northwestern Canada

2.1 Preface

The manuscript presented here will be submitted to a scientific journal in the upcoming year. Research objectives and the methodology used were co-developed by myself and my directors, Oliver Sonnentag and Manuel Helbig. I conducted all the data analysis in this study with the exceptions of the processing of eddy covariance data that were processed over the years by different members of the Laboratory in Atmospheric Biogeosciences in High Latitudes. All scripts related to data treatment and analysis were written by me. I used and adapted one script provided by my co-director Manuel Helbig to automatically download radiosonde data from Wyoming's Department of Atmospheric Science repository. The atmospheric boundary layer model was adapted from the original model available in python language on the GitHub repository of the CLASS model and translated to MATLAB. All results and figures were generated by me guided

by my directors to create figures that best illustrate my results. All the field work related to the deployment of weather balloons in the tundra was conducted by me. The article was written under the supervision of my directors who helped me with the structure and the quality of scientific writing.

2.2 Abstract

The circumpolar forest-tundra ecotone is experiencing changes in vegetation composition and structure and thus in surface properties (e.g., albedo) in response to climate change. Collectively, these changes in surface properties influence energy exchanges within the atmospheric boundary layer, potentially altering regional climate. Here, we showed how energy balance components and atmospheric boundary layer temperature and humidity varied across the forest-tundra ecotone in the Inuvialuit Settlement Region near Inuvik, NT in northwestern Canada. We used multi-annual, paired eddy covariance and supporting measurements made between 2013 to 2022 at a mineral upland tundra (Trail Valley Creek, TVC) and a nearby subarctic woodland site (Havikpak Creek, HPC) to characterize differences in surface properties and resulting energy partitioning. A mixed-layer slab model (Chemistry Land-surface Atmosphere Soil Slab, CLASS), in combination with radiosonde observations, was used to examine the implications of the sparse tree cover on the atmospheric boundary layer height, temperature and humidity. Compared to the treeless tundra, the sparse tree cover at HPC led to an enhanced ability to transfer heat into the atmosphere (indicated by larger aerodynamic conductance), a higher resistance to evapotranspiration (indicated by lower surface conductance) and a higher influence of atmospheric conditions on turbulent fluxes (indicated by a lower decoupling factor). Sensible heat (H) at HPC was generally higher than at TVC. The largest difference in daily mean H was observed in late winter and spring (March to May) when albedo of the snow-covered landscape at HPC was reduced by 45 % in comparison to TVC. Late winter and spring were characterized by more available energy at HPC (approximated by net radiation minus ground heat flux). Air temperature in the mixed layer computed with CLASS was up to 10 °C higher in spring and 3 °C higher in summer (June to August) at HPC than at TVC, respectively. Similar to the model results obtained with CLASS, radiosonde observations indicated a higher atmospheric boundary layer and higher temperature at HPC than at TVC. The presence of trees in the southern part of the forest-tundra ecotone has a warming effect on air temperatures throughout the year and a drying effect in spring.

2.3 Introduction

Considering its vast extent, the Arctic-boreal region plays an important role in the global climate system through its exchange of energy and matter with the atmosphere (McGuire et al., 2006). Air temperature across the Arctic-boreal region has been increasing at disproportionately high rates compared to the global average (Rantanen et al., 2022). Associated with climate warming, altered precipitation patterns (Hinzman et al., 2005), increased atmospheric carbon dioxide (CO_2) concentrations (Zhu et al., 2017), and intensified disturbance regimes (Foster et al., 2022) have led to changes in vegetation composition and structure across the Arctic-boreal region (Helbig et al., 2016; Myers-Smith et al., 2011; Ueyama et al., 2020; Wang et al., 2020). The Arctic-boreal region includes the forest-tundra ecotone (FTE), spanning more than 10,000 km across the northern hemisphere (Callaghan et al., 2002). As the world's longest transition zone, the FTE separates the boreal and Arctic biomes over a width of only a few hundred kilometers (Timoney and Mamet., 2020). Vegetation and thus ecosystem composition and structure vary considerably across the FTE as trees become, from south to north, shorter and stunted, sparser, and eventually, absent. The associated latitudinal gradient in surface properties results in corresponding latitudinal variations in how the FTE exchanges energy and matter with the atmospheric boundary layer (ABL). For example, in Alaska an increasingly sparser boreal forest tree cover dominated by "dark" black spruce (*Picea mariana*) transitions into "bright" Arctic tundra ecosystems, increasing the albedo (Beringer et al., 2005).

The net ecosystem exchanges of energy and matter with the atmosphere can be measured quasi-continuously with the eddy covariance technique (Baldocchi et al., 1988). Only a few studies have examined surface-atmosphere exchanges in the FTE with the eddy covariance technique (Lafleur and Rouse, 1995, Beringer et al., 2005). For example, Lafleur and Rouse (1995) compared turbulent fluxes of latent heat (LE) and sensible heat (H) between a boreal forest stand and a wetland tundra in the FTE of the Hudson Bay Lowlands during the summers of 1989 to 1993 (June to August). There, H and LE were respectively larger and smaller over the boreal forest stand than over the tundra wetland. Using eddy covariance measurements made at five sites across the FTE on the Seward Peninsula in western Alaska, Beringer et al. (2005) found a similar decrease in H and increase in LE from the boreal forest stands to the Arctic tundra sites.

In-situ and remote sensing observations, and projections with global dynamic vegetation models have suggested a shift of the FTE in some parts of the circumpolar Arctic-boreal region (Berner & Goetz, 2022; Gonzalez et al., 2010; Harsch et al., 2009; Pearson et al., 2013; Scheffer et al., 2012; Zhang et al., 2013). This shift is commonly manifested by densification and/or the northward encroachment of trees and/or taller shrubs (Tape et al., 2006). Positive trends in spectral indices from satellite data have been interpreted as 'Arctic greening', attributed to an increase in aboveground biomass and/or productivity (Goetz et al., 2005). In contrast, negative trends in spectral indices (i.e., 'Arctic browning') have been reported for other parts of the Arctic-boreal region (Phoenix & Bjerke, 2016). These opposite trends highlight the complexity in interpreting observations and projecting vegetation redistributions across the Arctic-boreal region in a circumpolar context. Some studies support the advancement and biome shift of the FTE into the tundra over the 20th century around the circumpolar north (Berner & Goetz, 2022; Harsh et al., 2009; Rees et al., 2020). Others observed modest to non-significant increase in tree cover in northwestern Canada and no significant evidence of northward migration of trees across subarctic central and western Canada since 1960 (Timoney & Mamet, 2020).

Western Inuit Nunangat is among the most rapidly warming regions of the Earth (Chylek et al., 2022; Rantanen et al., 2022). The recruitment of taller and more productive shrubs but not trees have been witnessed across the FTE in the Inuvialuit Settlement Region near Inuvik, NT (Lantz et al., 2012). The widespread shrub encroachment affects, for example, snowpack characteristics and distribution (Lantz et al., 2010), and thus the underlying permanently frozen ground (permafrost; Gruber, 2012) and ecosystem services including access to travel routes across the land and traditional livelihoods (Gibson et al., 2021). To better understand the impacts of potential vegetation distribution and composition changes on climatic conditions across the FTE, a better characterization of land-surface atmosphere interactions is needed. Surface-atmosphere energy exchange, ABL dynamics and characteristics across the rapidly changing FTE remain poorly understood.

Here, we synthesized multi-annual eddy covariance and supporting measurements (2013 to 2022) from two nearby eddy covariance tower sites (ca. 50 km apart) representing the FTE in the Inuvialuit Settlement Region (**Fig. 2.1**): a subarctic woodland ('woodland') and a mineral upland tundra ('tundra') near Inuvik, NT. The goal of this study was to develop a baseline understanding of the latitudinal variation in surface-atmosphere energy exchanges and surface climatic conditions

across the FTE in northwestern Canada. To meet this goal, our objectives were to 1) quantify seasonal differences in woodland and tundra energy exchanges, 2) examine bulk surface parameters to explain drivers of energy exchange differences, and 3) quantify the effects of woodland and tundra energy partitioning on ABL dynamics with a mixed-layer slab model and radiosonde observations. Characterization of baseline surface-atmosphere interactions is needed to develop a predictive understanding of tree or shrub densification and/or encroachment on regional climate in the circumpolar Arctic-boreal region.

2.4 Methods

2.4.1 Study sites

Paired eddy covariance and supporting measurements were made at two long-term research sites: Havikpak Creek (HPC; 68° 19' 13.3" N 133° 31' 7.4" W), a subarctic woodland site located ca. 10 km south of Inuvik, NT in the northern part of the Taiga Plains ecozone, and Trail Valley Creek (TVC; 68° 44' 31.29" N, 133° 29' 56.87" W), a mineral upland tundra site located ca. 40 km north of Inuvik, NT in the southern part of the Southern Arctic ecozone (**Fig. 2.1**). The close proximity of the study sites accounts for any potential variations in large-scale climate conditions. HPC can be characterized as a subarctic woodland on undulating, hummocky terrain mostly formed by moderately well-drained glacial till and overlain by silty clay and a thin organic layer (Eaton et al., 2001). The vegetation at HPC comprises scattered, stunted, mostly mature (> 70 years old) black spruce (*Picea mariana*) trees. HPC is predominantly covered by forest (>50.0%) followed by alder shrubs, short grass, moss and lichen tundra. Using a Plant Canopy Analyzer (LA-2200, LI-COR Biosciences Inc., Lincoln, NE) following methods described elsewhere (Ryu et al. 2010; Sonnentag et al., 2007a, b), mean (+/- one standard deviation) optically measured overstory and understory leaf area index (LAI) is 0.34 (+/- 0.16, n = 40) and 0.51 (+/- 0.19, n = 40), respectively.

Trail Valley Creek is a mineral upland tundra on slightly undulating, hummocky terrain of similar glacial origin as HPC, and incised by several narrow river and creek valleys. The low-stature tundra vegetation (<0.3 m in height, LAI = 0.35 [+/- 0.24, n = 54]) at TVC comprises dwarf shrubs (e.g., birch [*Betula nana, Betula glandulosa*], alder [*Alnus sp.*], willows), grasses and tussocks (cotton grass [*Eriophorum spp.*]), and patches of lichen and mosses. In addition, the surrounding lake-rich landscape at TVC also includes several periglacial tundra landforms and

associated cover types including ice wedges and polygons and barren ground. Both HPC and TVC are underlain by continuous permafrost (i.e., >90 % in areal extent; Gruber, 2012). Detailed site descriptions for HPC and TVC can be found elsewhere (e.g., Eaton et al., 2001; Krogh & Pomeroy, 2018; Marsh & Pomeroy, 1996; Wallace & Baltzer, 2019; Wilcox et al., 2019).

The climate of the Inuvik region is subarctic with short, warm to cool summers (June to September) and long, cold winters (October to May) (Beck et al., 2018). For the period 1981-2010, mean annual air temperature (MAAT) was -8.2 °C and mean annual total precipitation (MATP) was 240 mm at HPC. For comparison, TVC is generally colder and drier than HPC with MAT of -8.9 °C and MATP of 204 mm for the same period (McKenney et al., 2011). (McKenney et al., 2011).

Ca. 65 % of MATP falls as snow. Over the study period, (2013-2022), both HPC and TVC experienced similar variations in mean monthly air temperature and mean monthly total precipitation (**Fig. S1**). None of the study years was characterized by extreme air temperature or precipitation anomalies (defined as years with air temperature or precipitation anomalies exceeding more than two standard deviations from the climate normal, 1991-2020). Both regions have become significantly warmer (increased MAT) since 1980 (**Fig. S2**). Since 1980, mean annual air temperature has increased by 0.6 ± 0.3°C per decade while winter (mid-October to mid-March) air temperature has increased more rapidly at 0.9 ± 0.3°C per decade for both sites.

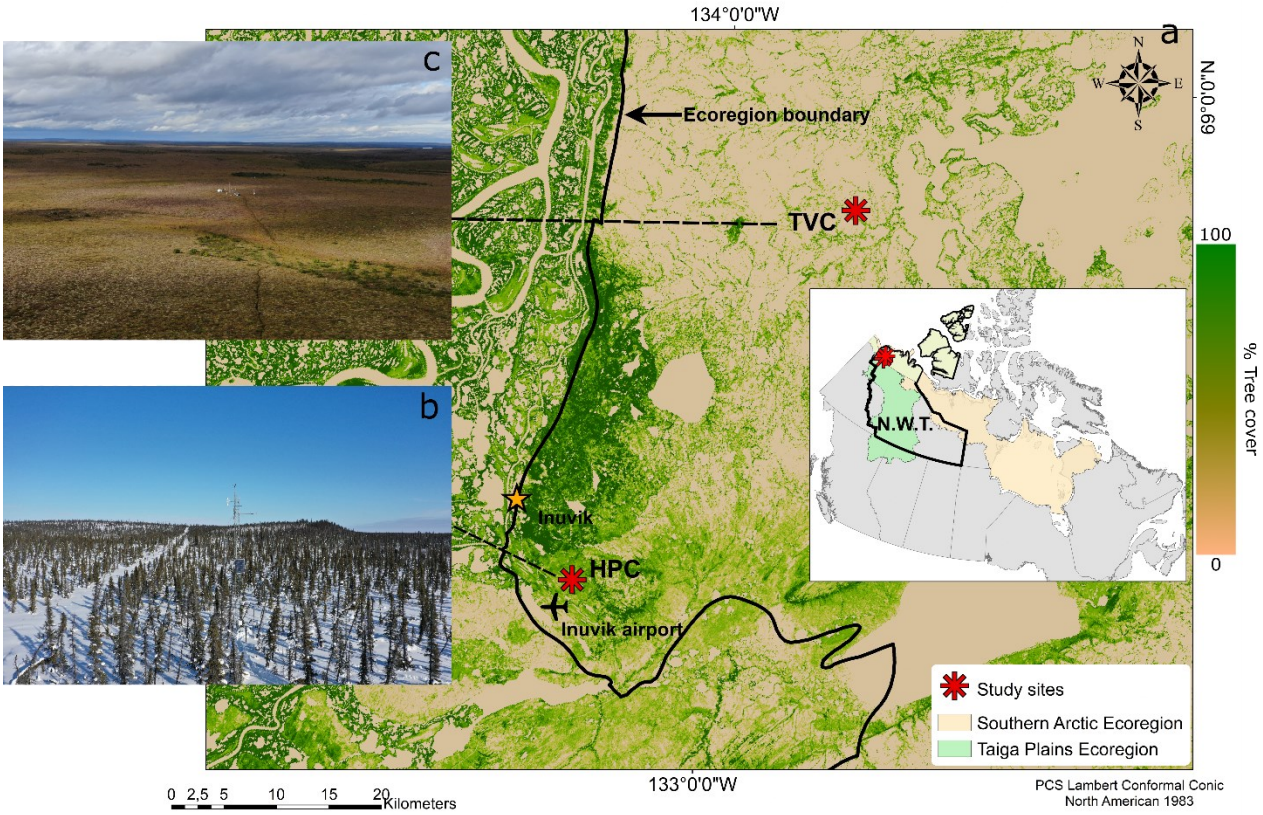

FIGURE 2.1 - a) Location of the two study sites characteristic of the forest-tundra ecotone between the Taiga Plains and Southern Arctic ecozones of northwestern Canada: b) Havikpak Creek (HPC, subarctic woodland) and c) Trail Valley Creek (TVC, mineral upland tundra), respectively. The backdrop map is the Global 2010 Tree Cover product (Hansen et al., 2013).

2.4.2 Eddy covariance and supporting measurements

Turbulent momentum and energy fluxes were measured using the eddy covariance technique (Baldocchi et al., 1988). The eddy covariance systems at TVC and HPC comprised identical three-dimensional sonic anemometers (CSAT3A; Campbell Scientific Inc., Logan, UT) and open-path infra-red gas analyzers (EC150; Campbell Scientific Inc.) to measure high-frequency fluctuations (10 Hz) in vertical wind velocity, and carbon dioxide and water vapour densities. Mounted on horizontal booms on triangular tower structures at 11.8 m (HPC) and 4.0 m (TVC) above the mean ground surface, the measurement heights provided sufficient fetch (several hundred metres) in all directions. Thus, flux footprints covered representative subarctic woodland (HPC) and mineral upland tundra source areas (TVC). Micrometeorological and eddy covariance instruments were controlled and logged using CR3000 data loggers at both sites (Campbell

Scientific Inc.). The eddy covariance systems were generally serviced twice a year, before snowmelt in late winter (April) and in late summer (August). Servicing consisted of performing routine maintenance as described in the EC150 user documentation, and water vapour zero and span calibration using gas standards and a dew point generator (LI-610; LI-COR Biosciences Inc.). The TVC time series has a data gap from November 2014 to August 2015 due to instrument failure. Both TVC and HPC tower structures were deemed unsafe to climb in early 2014. Replacement tower structures were constructed in 2015 at HPC and August 2016 in TVC, and reinstrumented in August 2016, replicating the original instrumental set-up (i.e., height, orientation). Consequently, the HPC time series has a data gap from December 2013 to August 2016.

Half-hourly turbulent fluxes of latent heat (LE, W m^{-2}) and sensible heat (H, W m^{-2}) were calculated using the EddyPro software package (version 7.0.6; LI-COR Biosciences Inc). Details on the data processing are provided elsewhere (Helbig et al., 2016, 2017). At both sites a double-rotation method was applied to rotate the coordinate system of the sonic anemometer into the mean streamlines of the wind field (Wilczak et al., 2001). We removed spikes in the high-frequency time series (Vickers & Mahrt, 1997), corrected fluxes for spectral attenuation (Moncrieff et al., 1997), and accounted for air density fluctuations (Webb et al., 1980) and humidity effects (Van Dijk et al., 2004). Storage fluxes were calculated using the one-point method, which consists in calculating temporal changes of the concentrations measured at the tower top and assuming a constant concentration in the air column underneath.

Finally, we applied a three-class quality flag system to retain only high-quality data for analysis (i.e., quality flags 0 and 1; Mauder & Foken, 2011). Any remaining outliers in the half-hour time series were filtered using a spike-detection algorithm and fluxes during periods with friction velocity below 0.1 ms^{-1} were removed as suggested by Papale et al. (2006). Turbulent fluxes were gap-filled using the Marginal Distribution Sampling algorithm described in Reichstein et al (2005). Remaining long winter gaps were filled with mean half-hour averages for the same days and hours in the remaining years. All analyses were done on daily LE and H for "good" days defined as days for which less than 24 half hours were missing (i.e., <50 %).

Net radiation (Rn, W m^{-2}) at HPC and TVC was measured using four-component net radiometers (HPC: CNR1, TVC: CNR1 2012 to Aug 2019 and CNR4 Aug-2019 onwards; Kipp and Zonen, Delft, the Netherlands) installed on south-facing booms at 11.8 m and 4.08 m above the mean ground surface, respectively. Soil heat flux (G, W m^{-2}) was calculated using ground heat

flux plates, soil temperature probes, and soil moisture probes (HFT3 [Hukseflux, Delft, the Netherlands], TCAV and CS616 [both Campbell Scientific Inc.]) at 8 cm below the ground surface (HPC) and at 5 and 9 cm below the ground surface (TVC) (from the ground surface, organic and mineral layers, respectively). Soil heat flux at TVC was estimated as the mean of mineral and organic soil heat fluxes. Soil energy storage terms for the soil layer between the ground surface and the depth of the heat flux plates were calculated by calculating the organic/air/water fraction of soil and calculating energy stored per change in temperature. Air temperature (T_{AIR}, °C) and relative humidity (RH, %) were measured at 13.8 m (HPC) and 4.6 m (TVC) using temperature-humidity probes (HC2S3; Campbell Scientific Inc.). Tower-based potential temperature (θ, °C) and specific humidity (q, g kg^{-1}) were calculated with T_{AIR}, air pressure and RH.

Energy balance closure was calculated as the regression slope of the daily sum of half-hourly turbulent fluxes [H + LE] and available energy [Rn - G] during the summer (June-July-August). Winter and shoulder seasons, spring and fall, were excluded to minimize uncertainties introduced by additional energy balance terms (e.g., snow melt, melt energy from soil ice). Energy balance closure was 0.90 and 0.74 at TVC and HPC, respectively.

2.4.3 Mixed-layer slab model

To quantify the effects of woodland (HPC) and tundra (TVC) surface fluxes on ABL dynamics, we used a mixed-layer slab model (Chemistry Land-surface Atmosphere Soil Slab model [CLASS]; Vila-Guerau de Arellano et al., 2015). CLASS is based on the assumption that θ, q, and wind components are constant within the mixed layer. Changes of θ and q within the mixed-layer result from the combined effects of surface and entrainment fluxes of H and LE (Vila-Guerau de Arellano et al., 2015). We used CLASS to simulate diurnal and seasonal changes in ABL dynamics as described by daily estimates of afternoon ABL height (ABLH), and mixed layer θ and q, obtained with CLASS and the contribution of surface and entrainment fluxes to θ and q. The model was forced with half-hourly gap-filled H and LE from 5:00 MST and 17:00 MST, corresponding to early morning and late afternoon launch times of operational radiosondes from the Inuvik Upper Air Weather Station (ca. 700 m south-east of HPC). A detailed description of CLASS is given by others (Tennekes, 1973; Tennekes & Driedonks, 1981; van Heerwaarden and Teuling, 2014; Vila-Guerau de Arellano et al., 2015).

The Chemistry Land-surface Atmosphere Soil Slab model requires initial estimates of jumps in potential temperature and specific humidity at ABLH, lapse rates of potential temperature and specific humidity in the free atmosphere, and initial θ and q in the mixed-layer. Initial estimates of θ and q jumps at ABLH were set the same at TVC and HPC and defined as the difference between θ and q at the ABLH and their means within the mixed layer as derived from afternoon radiosonde observations. Lapse rates in the free atmosphere were estimated as the slope parameter of linear regressions of height on θ and q (from 5am radiosonde profiles) using measurements from all levels between 1000 m and 6000 m above ground as in Helbig et al. (2020) and were kept constant throughout the day. Initial θ and q in the mixed layer were set using tower-based measurements at 5a.m. The effect of large-scale subsidence velocity on ABL growth was evaluated and calculated using hourly horizontal divergence (s^{-1}) from ERA5 reanalysis (Hersbach et al., 2023) at 750 hPa (~ 2500 m above the ground; around the maximum ABL height) but was found to be negligible. The effect of wind shear at the surface was not considered in the calculation of the entrainment velocity. The model was run for cloudy and clear-sky days. Cloudy days were defined as days with less than 70% of daily potential solar radiation expected for the latitude. Daily potential solar radiation for the latitude was calculated in the R computing environment (v4.0.3; R Core Team 2020) using the "potential.radiation" function from the R package 'bigleaf' (v0.8.2, Knauer et al., 2018).

2.4.4 Radiosonde observations

Daily estimates of ABLH, and mixed layer θ, and q at HPC obtained with CLASS were evaluated against corresponding radiosonde estimates made at the Inuvik Upper air Weather Station near HPC. We used operational radiosonde data from the Inuvik Upper Air Weather Station from the University of Wyoming's Department of Atmospheric Science repository (http://weather.uwyo.edu/upperair/sounding.html). Sounding data were filtered to keep only soundings showing a well-defined mixed-layer and unstable or neutral atmospheric conditions. Thus, soundings with constantly increasing θ with altitude were discarded, indicating stable atmospheric conditions. To ensure the presence of a well-mixed layer, radiosonde θ profiles with a standard deviation higher than 1 K in the mixed layer were also discarded. Only days with both available morning and afternoon soundings and matching days with high-quality surface flux observations were used. The atmospheric boundary layer height was derived for afternoon profiles

using the parcel method with an excess temperature of 1 K added to the first measurement height near the surface (Holzworth, 1964; Seibert, 2000). An excess temperature was applied to ensure the representation of a superadiabatic layer near the ground that was often missing, especially when the first measurement in the radiosonde profile was well above the ground. The lowest measurement was often at 0 meters above ground but extended to 20 to 200 meters in some cases. The atmospheric boundary layer height was defined as the first height measurement at which radiosonde θ is equal to or is higher than radiosonde θ at the surface (Seidel et al., 2010).

Additionally, radiosonde observations from two summer campaigns at TVC in early June 2021 and late August 2022 were used for comparison with corresponding estimates obtained with CLASS at TVC (Fig. S3). High-resolution (1 m) reusable radiosondes (Sparv Embedded AB, Linkoping, Sweden; Bessardon et al., 2019) were launched with twelves launch at around 17:00 MST when clear sky conditions were present (**Fig. S4**). Out of 40 radiosonde launches, three matched with days with high-quality surface flux observations suitable for forcing CLASS. Radiosondes were generally dropped between 1 and 2 km above the ground surface to allow their recovery on foot. Radiosonde observations at TVC were also compared to radiosonde observations at HPC made at the Inuvik Upper Air Weather Station.

2.4.5 Analysis

We defined distinct seasons (winter, spring, summer, fall) based on pooled Rn measurements made at HPC and TVC. Using daily mean Rn across years (2013 - 2022), the start of winter was defined when Rn < 0 W m-2, start of spring and fall when Rn > 0 W m-2 and start of summer when Rn >= 100 W m-2 for three or more consecutive days (Oechel et al., 2014). In addition, winter was further subdivided into 'early winter' (i.e., from the start of winter to the end of the year) and 'late winter' (i.e., from the start of the year to the end of winter). The mean ()2013-2022) of the site-specific day-of-year (DOY) of the start of each season was used as the season definition for the FTE in the Inuvialuit Settlement Region.

To shed light on daily, and seasonal differences (spring, summer, fall) in woodland (HPC) and tundra (TVC) surface energy exchanges (TVC), we examined six key bulk surface parameters (Baldocchi & Ma, 2013; Beringer et al., 2005; Helbig et al. 2016; Helbig et al., 2020; Ryu et al., 2008) : albedo (**α**, unitless; Stephens et al., 2015), aerodynamic conductance (Ga, m s^{-1-1}; Thom., 1972), surface conductance (Gs, m s-1-1; Monteith., 1965), decoupling factor (**Ω**, unitless; Jarvis

& McNaughton, 1986) which indicates the degree of coupling between the land surface and the atmosphere, ranging from 0, when evapotranspiration is controlled by Gs and vapor pressure deficit, to 1 when evapotranspiration is controlled by Rn, Bowen ratio (BR), and evaporative fraction (EF). Using high-quality half-hourly fluxes of H and LE from 12:00 MST to 16:00 MST, i.e., two hours before to two hours after solar noon), the six bulk surface parameters were calculated using the R package 'bigleaf' (v0.8.2, Knauer et al., 2018). After discarding outliers in half-hourly bulk surface parameters estimates based on visual inspection, median daily bulk surface parameters were calculated. Average daily spring, summer and fall bulk surface parameters for HPC and TVC were tested for significant differences with the Wilcoxon rank-sum test ($\alpha = 0.05$).

The performance of CLASS to reproduce ABL dynamics at HPC was assessed, first, qualitatively by comparing modelled mean (2013-2022) afternoon ABLH, and modelled diurnal changes in atmospheric boundary layer θ, (Δθ) and q (Δq), calculated as the difference between modelled θ and q at 17:00 MST and initial θ and q at 5:00 MST, respectively, to corresponding estimates from the radiosonde observations at HPC. Every day, radiosonde estimates of Δθ and Δq were calculated as the difference between afternoon (17:00 MST) profile mean θ and q and the near surface θ and q from the morning profiles (5:00 MST), respectively. Daily contributions of surface and entrainment H and LE to modelled Δθ and Δq were estimated as the cumulative sum of half-hourly observed surface and modelled entrainment H and LE fluxes at HPC and TVC. Second, we used orthogonal linear regression and associated metrics (coefficient of determination [R2], mean average error [MAE]) to assess the skill of CLASS to reproduce daily radiosonde estimates of ABLH, Δθ, and Δq between 2013 and 2022.

2.5 Results

2.5.1 Surface-atmosphere energy exchanges

Differences in mean daily LE across years (2013-2022) between HPC and TVC were small (<10 W m^{-2}) with LE peaking at around 50 ± 30 W m^{-2} (± one standard deviation) at HPC and TVC in July (**Fig. 2.2a**). Latent heat flux was low (<10 W m^{-2}) in early spring when air temperature was still below the freezing point. In contrast, mean daily H was around 33 ± 15 W m^{-2} at HPC compared to -4 ± 18 W m^{-2} at TVC in spring (**Fig. 2.2b**). The difference in H was smaller in early summer when H peaked at 80 ± 20 Wm^{-2} at HPC and at 70 ± 23 Wm^{-2} at TVC. Differences in H

between the two sites were small (<10 W m^{-2}) in fall. At both sites, H peaked about 30 days earlier than LE, i.e., in early June versus early July.

Mean daily R_n across years (2013-2022) was generally higher at HPC than at TVC in late winter and spring, reaching a maximum difference of 53 W ± 14 W m^{-2} in spring (**Fig. 2.2c**). The lowest difference in R_n was observed during the summer and fall when R_n at HPC was higher by 17 ± 17 W m^{-2} compared to TVC. Differences in outgoing shortwave radiation (SW_{out}) were the main cause of differences in R_n (**Fig. S5**), indicating that albedo differences were mainly responsible for differences in R_n. Mean daily G at TVC peaked at 51 ± 24 W m^{-2} in early summer (**Fig. 2.2d**) and peaked 30 days later at 8.5 ± 2 W m^{-2} at HPC. Ground heat flux was slightly negative until late spring at both sites and amounted to around 12 ± 6W m^{-2} in fall at TVC and 3 ± 1 W m^{-2} at HPC.

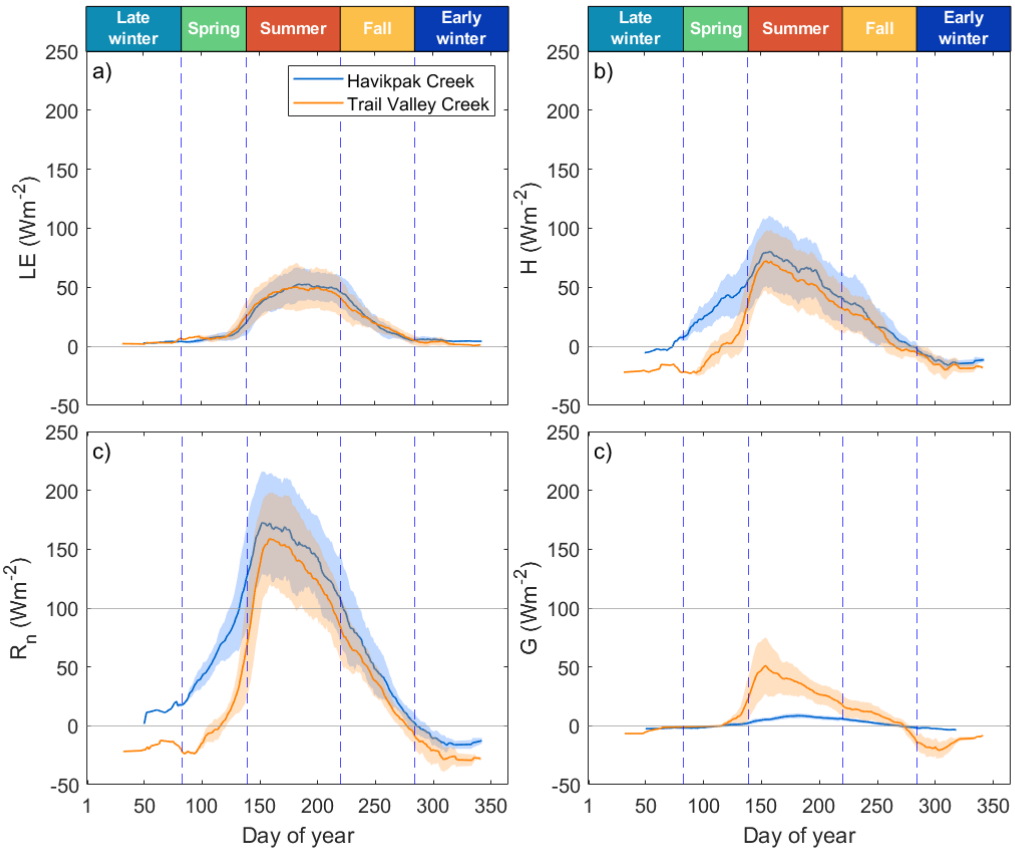

FIGURE 2.2 - Fourteen-day moving averages of energy balance components across all years (2013-2022): a) latent heat flux (LE), b) sensible heat flux (H), c) net radiation (Rn) and d) ground heat flux (G) at Havikpak Creek (woodland) and Trail Valley Creek (tundra). Vertical dashed lines indicate the beginning and end of different seasons. Shaded areas indicate the standard deviation across years.

2.5.2 Bulk surface parameters

The EF was consistently higher at TVC than at HPC and was increasing from spring to summer at both sites while fall EF was similar to summer (**Fig. 2.3a**). The partitioning of available energy at HPC changed rapidly during spring indicated by a steep decrease in BR (**Fig. 2.3b**). The Bowen ratio decreased from spring to fall, being around 4.25 and 1.32 in spring and 1.66 and 1.31 in fall at HPC and TVC, respectively. During all seasons, the EF was higher and BR lower at TVC than at HPC. As indicated by significantly higher Ga, the efficiency to exchange heat with the atmosphere was higher at HPC than at TVC (**Fig. 2.3c**). In contrast, Gs was generally higher at TVC than at HPC (**Fig. 2.3d**). A higher **Ω** at TVC indicates that the tundra was less well coupled to the atmosphere than HPC (**Fig. 2.3e**). Daytime median values of the **Ω** were 0.07 and 0.24 in spring, 0.21 and 0.35 in summer, and 0.23 and 0.38 in fall for HPC and TVC, respectively. Both HPC and TVC are more coupled to the atmosphere in spring than in the other seasons. A large difference in **α** was observed in spring, when TVC reflected about 45 % more of incoming shortwave radiation than HPC with a median **α** of 0.51 at HPC compared to 0.82 at TVC (**Fig. 2.3f**). With snowmelt, **α** decreased rapidly and was similar in summer and fall with around 0.20 for TVC and 0.12 for HPC.

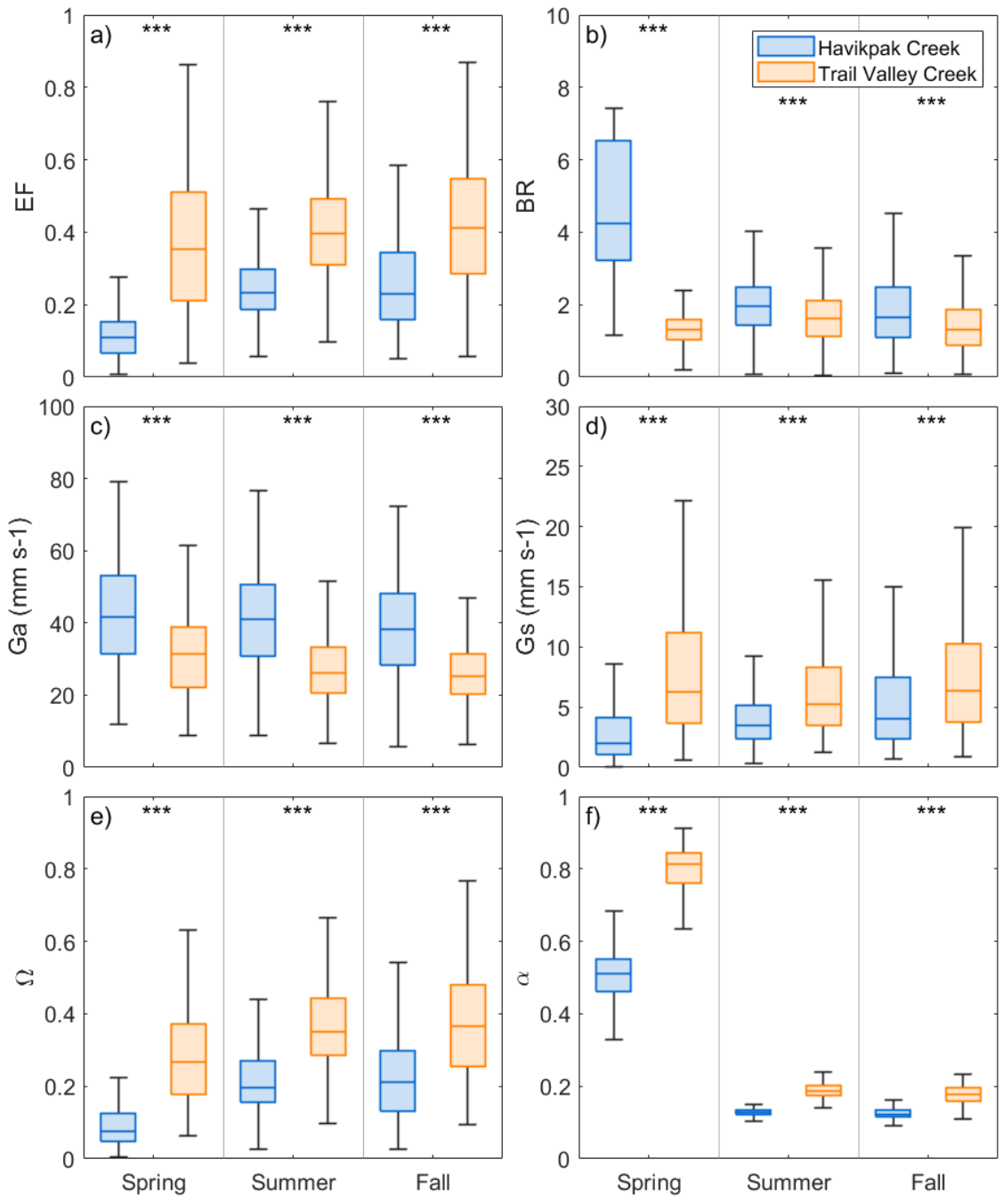

FIGURE 2.3 - Differences in seasonal median of daily a) evaporative fraction, b) Bowen ratio, c) aerodynamic conductance (Ga, mm s-1), d) surface conductance (Gs, mm s-1), e) decoupling factor (**Ω**, unitless), and f) and albedo (**α**, unitless) at Havikpak Creek (woodland) and Trail Valley Creek (tundra) between 2013 and 2022. The asterisk (*) indicates the significance-level of the Wilcoxon rank sum test at α = 0.05: p-value < 0.05 (*), p-value < 0.01 (**), and p-value < 0.001 (***). The bottom and top of each box are the 25th and 75th percentile with the middle line representing the median. Whiskers are the minimum and maximum non-outlier values.

2.5.3 Atmospheric boundary layer dynamics

The subsequent results section focuses on the characterization of near-surface conditions, using tower-based measurements at HPC and TVC. This is followed by an evaluation of CLASS against radiosonde observations at HPC, providing valuable insights into the model's performance. The section then proceeds to present the simulation results for both HPC and TVC.

Mean daily (2013-2022) tower-based θ at HPC was generally higher than at TVC throughout the year with the maximum difference between HPC and TVC reaching 2.7 ± 1.9 °C in spring (**Fig. 2.4a**). In spring and summer, tower-based θ at HPC and TVC were significantly different, but not in fall (**Fig. 2.4b**). In contrast, mean daily (2013-2022) tower-based q differences between HPC and TVC were small (< 0.1 g kg^{-1}) with a large variability in summer (± 0.7 g kg^{-1}) (**Fig. 2.4c)**. Specific humidity near the surface was not significantly different in summer and fall with a relatively weak difference in spring. (**Fig. 2.4d**).

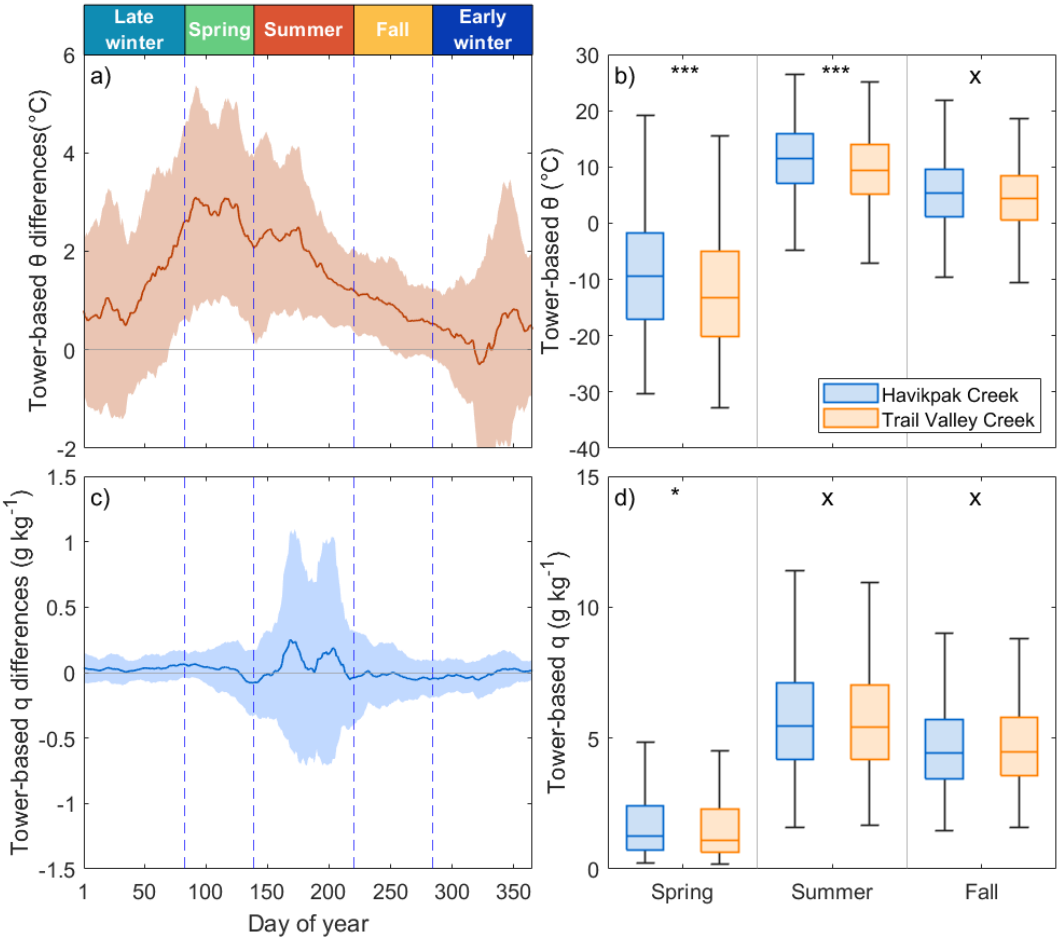

FIGURE 2.4 - a) Differences (HPC minus TVC) in 14-day moving average of mean (+/- one standard deviation [std]) daily tower-based potential temperature at Havikpak Creek (θ, °C) and at Trail Valley Creek across all years (2013-2022), b) seasonal median of daily tower-based θ, c) differences in 14-day moving average of mean (+/- std) daily tower-based specific humidity (q, g k-1) across all years (2013-2022), and d) seasonal median of daily tower-based q. The asterisk (*) indicates the significance-level of the Wilcoxon rank sum test at $\alpha = 0.05$: p-value < 0.05 (*), p-value < 0.01 (**), and p-value < 0.001 (***).

A deeper ABL at HPC than at TVC was simulated over the entire year (**Fig. 2.5a**). The largest differences in modelled ABLH between HPC and TVC occurred in spring, with a mean (2013-2022) afternoon difference of around 880 ± 35 m. Differences between modelled ABLH at HPC and TVC were smaller in summer and fall with a mean difference of 155 ± 190 m. The ABL started to substantially grow at TVC only late in spring when H became positive. Differences between modelled afternoon mixed layer θ followed similar seasonal patterns as differences in modelled ABLH (**Fig. 2.5b**). The largest difference occurred in spring with modelled mixed layer θ being around 10.3 ± 0.72°C higher at HPC. Differences between modelled mixed layer θ at HPC

and TVC then gradually decreased to 3.1 ± 1.6°C on average in summer and 1.6 ± 0.35°C in fall. Modelled mean afternoon mixed layer q also showed the largest difference of -2.8 ± 0.6 g/kg in spring while differences in summer and fall were small and below 0.1 ± 0.3 g/kg (**Fig. 2.5c**).

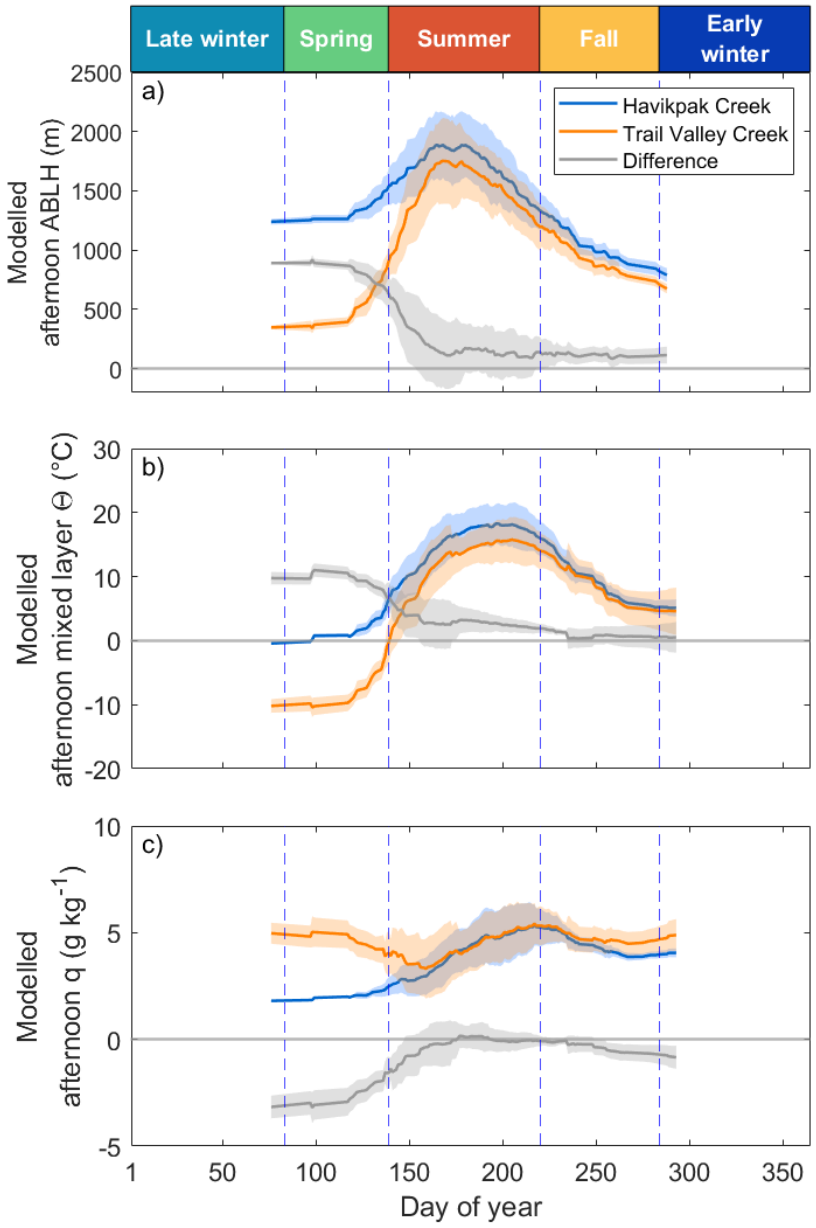

FIGURE 2.5 - Thirty-day moving averages in modelled (CLASS) a) afternoon atmospheric boundary layer height (ABLH), b) afternoon mixed layer potential temperature (θ) and c) afternoon mixed layer specific humidity (q) at Havikpak Creek and Trail Valley Creek across all years (2013-2022).

Diurnal changes in modelled potential temperature were significantly different in spring with median modelled Δθ at HPC increasing by around 5.6 °C and at TVC by 1 °C over the course of a day. Surface fluxes respond to moisture and heat entrained from the free atmosphere. Understanding contributions of surface and entrainment fluxes is crucial to explain differences in near surface climatic conditions between HPC and TVC. In spring, 70% of modelled Δθ at HPC was attributed to surface H while accounting for 5% at TVC. Both surface and entrainment H at HPC in the summer were slightly larger than at TVC leading to an increase of modelled Δθ by 7.8 °C at HPC and by 7.2°C at TVC. In fall, modelled Δθ at HPC and TVC were not significantly different, being respectively 5.6°C and 5.4°C. In summer and fall, surface H at HPC and TVC contributed to modelled Δθ to a similar extent, about two thirds in summer and fall. Overall, surface H at HPC and TVC contributed more to modelled Δθ than entrainment H. A decrease in modelled Δq at HPC by 0.2 g kg^{-1} and an increase in modelled Δq at TVC by 1 g kg^{-1} was simulated in spring. However, there is large variability in modelled Δq at TVC. Diurnal decrease in q was the largest in summer with no significant differences between modelled Δq at the two sites. In summer, drying from entrainment LE exceeded wetting from surface LE by around 0.7 g/kg and 0.4 g/kg at HPC and TVC, respectively. There was no significant difference between modelled Δq at HPC and TVC in fall when the drying effect diminished to 0.5 g kg^{-1} and 0.35 g kg^{-1}, respectively.

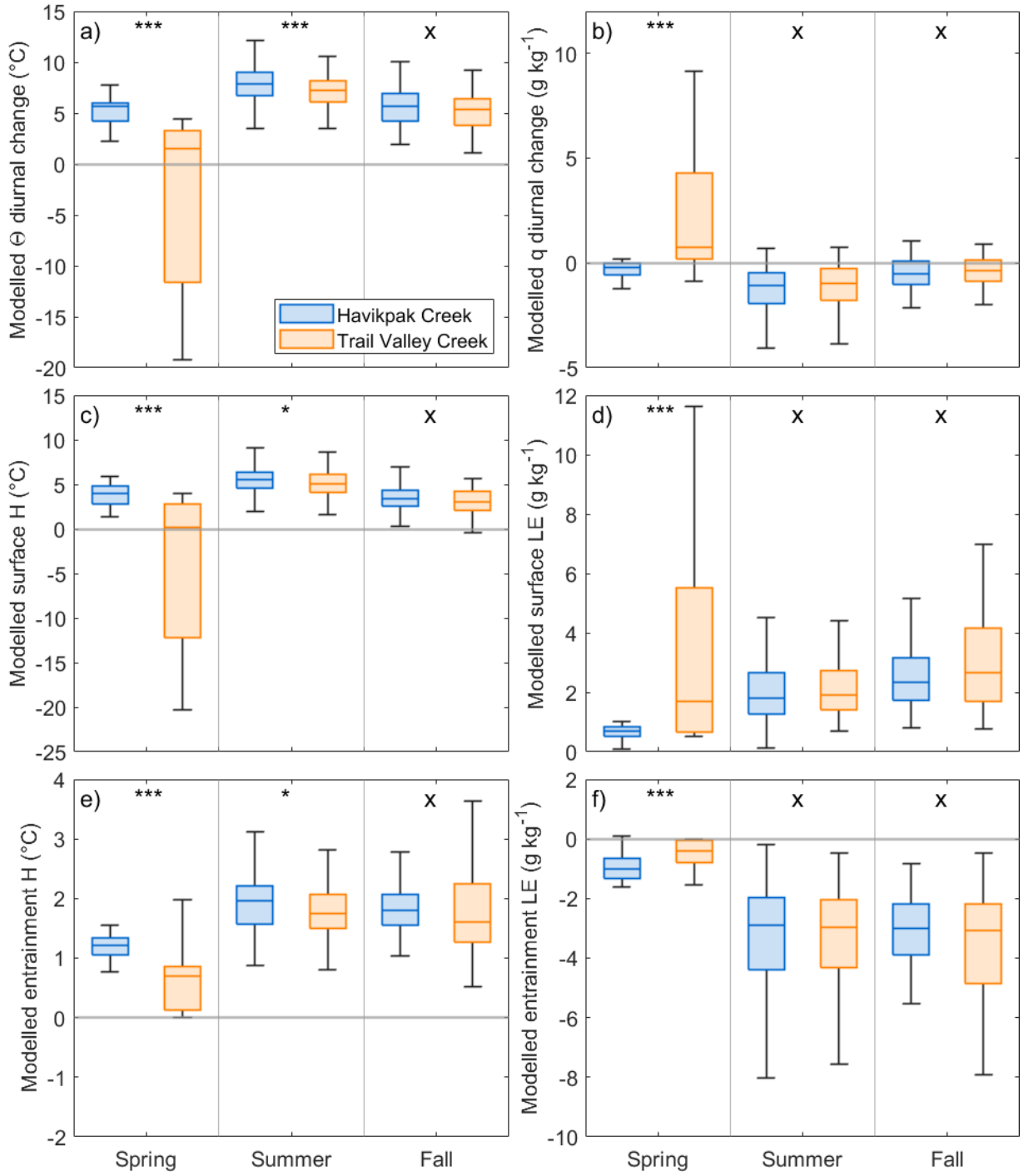

FIGURE 2.6 - Modelled diurnal changes in a) potential temperature (Δθ), b) specific humidity (Δq) and the contribution from c) surface sensible heat (H), d) surface latent heat, e) entrainment of sensible heat and entrainment of latent heat at Havikpak Creek and Trail Valley Creek across all years (2013-2022). The asterisk (*) indicates the significance-level of the Wilcoxon rank sum test at $\alpha = 0.05$: p-value < 0.05 (*), p-value < 0.01 (**), and p-value < 0.001 (***).

2.6 Discussion

In this study, we show that surface climate characteristics and ABL dynamics varies spatially across the FTE. Changes in the FTE distribution can therefore modify regional climate change pathways. However, observed and predicted FTE changes are complex and highly uncertain. Our results show a similar warming effect of increasing tree coverage in the mixed layer as reported by Helbig et al. (2016) and Ueyama et al. (2020). Enhanced tree coverage also leads to a deeper ABL and lower atmospheric moisture in spring. However, no significant differences in modelled q are shown in summer and fall.

2.6.1 Seasonal and spatial differences in woodland and tundra energy exchanges

In this study, we found H to dominate at HPC with a Bowen ratio being higher than at TVC throughout the year with the largest difference in spring. In spring, snow still covers the ground and trees mask the snow, resulting in a large difference in albedo and available energy. This period of large differences in available energy ends in early June after snowmelt. The resulting albedo and radiative differences in spring between tall and short canopy ecosystems have been reported for other northern regions (Baldocchi et al., 2000; Beringer et al., 2005; Lafleur & Rouse, 1995). In summer, albedo differences are smaller. However, darker tree canopies still result in lower albedo and larger available energy.

Frozen soil water in spring restricts plant root uptake of water in addition to chilling and freezing stress, overall leading to reduced stomatal conductance (Baldocchi et al., 2000; Teskey et al., 1984). Evapotranspiration is thus limited and explains the low LE flux at HPC and TVC until late spring. Latent heat flux then increased in summer with HPC and TVC experiencing similar LE flux. Beringer et al. (2005) found that the summer EF varied only slightly between 0.35 to 0.37 across a gradient of moist evergreen forest to a moist tundra on the Seward Peninsula in western Alaska. There, EF tended to be slightly lower at the tall shrub, woodland and forest sites relative to the tundra. We found a larger variability in EF between HPC and TVC with lower EF at HPC than at TVC. Both sites were also part of another comparative study from Eaton et al. (2001). They found lower summer EF at HPC than at TVC, consistent with our observations. However, reported EF by Eaton et al. (2001) was higher than in our study at both sites, around 0.53 for TVC and 0.46

for HPC. The different reported EF in this study could be explained by the multi-year averages reported here, which might cover a wider range of environmental conditions than the two-year dataset used by Eaton et al. (2001).

The similar LE flux, the higher Bowen ratio, and lower EF at HPC compared to TVC indicates that more energy was used to moisten the atmosphere at TVC, while more energy was used to warm the atmosphere at HPC. However, the Bowen ratio decreased from spring to fall while EF increases at HPC, indicating that more energy was used to moisten the atmosphere later in the growing season than early in the growing season. This pattern could partly explain the smaller modelled θ and q differences between HPC and TVC later in the growing season. At TVC, EF increased from spring to fall and the change in Bowen ratio indicated a shift from energy partitioning from H to LE.

2.6.2 Differences in surface properties across the forest-tundra ecotone

Bulk surface parameters such as Ga and Gs can be useful to explain how the surface properties of ecosystems control the partitioning of the energy. These surface parameters provide us with mechanistic information to diagnose how changes in air temperature and humidity could follow a vegetation shift (Baldocchi & Ma, 2013). For example, rougher surfaces, such as at the woodland site, increase Ga and enhance their ability to transfer mass and energy with the atmosphere (Jarvis & McNaughton 1986, Baldocchi et al., 2000). This could contribute to the larger H flux and deeper boundary layer in summer over HPC and similar LE despite a lower surface conductance. Increasing tree coverage then contributes to higher temperature and a higher ABL, with an enhanced ability to transfer heat into the atmosphere (Baldocchi & Ma, 2013).

The similar LE fluxes at HPC and TVC, along with a similar EF in the summer at both sites, are supported by findings by Beringer et al. (2005) and Thompson et al. (2004) in Alaska. This suggests that similar processes control the partitioning of the energy in our study region. With a significantly lower decoupling factor, HPC is more well coupled to the atmosphere than TVC, indicating that LE depends more on atmospheric conditions. Thus, atmospheric conditions like VPD rather than radiation control LE at HPC, which was characterized by a higher VPD. At TVC, Rn was more important in driving LE than at HPC with relatively unrestricted evaporation of with the low resistance to water loss of the vegetation (Baldocchi et al., 2000; Beringer et al., 2005). In the same way as Beringer et al. (2005), this suggests that tree densification and increases in stem

density, as observed across our FTE sites (Lantz et al., 2019; Travers-Smith & Lantz, 2020), has the potential to alter the sources and controls of LE, making water loss more sensitive to VPD (Beringer et al., 2005).

2.6.3 Atmospheric boundary layer dynamics

The ABL height is an important factor controlling regional climate dynamics. Surface fluxes exert a strong control on ABL growth, which affects air temperature and humidity through the entrainment of dry and warm air from the free atmosphere (Baldocchi & Ma, 2013; Denissen et al., 2021; Helbig et al., 2021; Vila-Guerau de Arellano et al., 2015). In order to fully understand land-atmosphere interactions across the FTE and to assess how potential vegetation changes would affect surface climatic conditions, changes in the surface energy balance need to be linked to ABL growth feedbacks.

At the FTE in northwestern Canada, the ABL shows important variations in height, mixed layer θ q between the forested-woodland and the tundra depending on the season. In spring, the large mixed layer θ difference can be explained by the large difference in H and the quasi-absence of LE to cool the air at HPC. The albedo difference and the resulting strong difference in Rn thus plays a major role in spring in determining surface climatic conditions. However, in summer and fall, a similar LE flux and small differences in H flux are found. Here, we argue that even small differences in H lead to different mixed layer θ.

Differences in mixed layer θ between HPC and TVC gradually decrease over the year as well as ABL height differences, while LE flux takes on importance and peaks in summer. At TVC, more of the available energy is used for the evapotranspiration, leading to a shallower boundary layer for the same surface input of water vapour as HPC.

Our results are similar to those of Helbig et al. (2016) and Ueyama et al. (2020) who showed that atmospheric moistening presumably occurred due to a decreased entrainment of dry air by decreased ABL height and increased LE. Here, the entrainment of dry air was not significantly different in summer resulting in similar moisture in the ABL. At both sites, the entrainment of dry air exceeded the surface input of humidity in summer, leading to a decrease in q over the course of the day in summer and fall. The modelled Δθ and Δq are similar to the tower observations made near the surface at HPC and TVC (**Fig. 2.5**). In both cases, the largest θ differences occur in spring, and then gradually decrease in summer and fall. However, differences in observed q at the towers

are not significant in spring near the surface while a significant difference between HPC and TVC is modelled in the ABL.

The boreal forest canopy exerts a significant resistance to evaporation and the open nature of the canopy at the FTE causes a large amount of energy exchange to occur at the soil surface. This low rate of evaporation causes high rates of H exchange and deep ABL that enhance the VPD through entrainment of dry air (Baldocchi et al., 2000). Here, we show that the increased aerodynamic conductance at HPC compensates for the lower surface conductance leading to similar LE at both sites. However, with slightly higher available energy and higher H at HPC and enhanced entrainment of dry air, an increase in tree cover at the FTE could enhance the drought stress on the vegetation and increase wildfire vulnerability (Sedano & Randerson, 2014). These potential changes in ABL height, mixed layer θ and q following vegetation shifts and their effect on regional precipitation patterns, cloud formation and carbon exchanges need further research (Vila-Guerau de Arellano et al., 2015).

2.6.4 Limitations of the study

The causes of the overestimation of the ABL height in this study remain unclear. Contributing to the discrepancies could be the vertical resolution of the radiosonde profiles that varied from 20 meters near the surface to 300 meters around the ABL height. Also, the parcel method highly depends on surface θ to identify the ABL height and the estimated ABL height value may vary substantially in situations without a pronounced θ inversion at the ABL top (Seibert et al., 2000). For example, when θ is slightly increasing with height in the mixed layer under slightly stable atmospheric conditions, an underestimation of the ABL height can occur. Observations of θ used to evaluate the model were made at the Inuvik Upper Air Weather Station (ca. 700 m south-east of HPC), where conditions at the surface are different than at HPC. While surface θ at the two locations were in good agreement, some differences were present and could have influenced the estimation of the ABL height. Other methods were tested like the Richardson number method, which resulted in similar results to the parcel method.

Model simulations showed relatively large discrepancies with observations in spring when local climate conditions differed the most. With large spatial gradients in θ and q, horizontal advection could play an important role in ABL dynamics (Pal et al., 2021). In this study, we did not include horizontal advection terms due to the lack of supporting ground observations. The

advection of temperature and humidity could play a role in shaping surface turbulent fluxes and therefore influence ABL development (Porter et al., 2018). The Mackenzie Delta, situated approximately 15 km northwest of the Inuvik Airport, could play an important role in local climate conditions by bringing additional moist air of the region (Porter et al., 2018). Future studies focusing on mesoscale circulation induced by spatial gradients in θ and q could provide important insights into regional climate dynamics in the region.

Neglecting the mechanical turbulence term in CLASS caused by wind shear (u*) at the surface had an effect on simulated ABL height since both sites are characterized by different surface roughness. However, modelled ABL height calculated using u* led to even more pronounced overestimation of ABL heights.

Differences in energy balance non-closure at eddy covariance flux tower sites may be attributed to underestimation of ground heat flux, particularly considering the open canopy at HPC. The mean daily summer G/Rn (global radiation/net radiation) across all years (2013-2022) was 0.04 at HPC. In comparison, Beringer et al. (2005) reported a daily G/Rn of 0.10 for a woodland, and Eugster et al. (2000) reported G/Rn of 0.06 for a treeline forest. Similarly, at TVC, ground heat flux might be overestimated, as the mean daily summer G/Rn across all years (2013-2022) was 0.26. For a tundra environment, Beringer et al. (2005) found a G/Rn of 0.12, while Eugster et al. (2000) reported G/Rn ranging between 0.10 and 0.24 for similar tundra environments. As the imbalance cannot be solely attributed to turbulent fluxes, we have decided not to correct the imbalance at both sites. Underestimated turbulent fluxes at HPC could lead to underestimated differences in surface climatic conditions and ABL dynamics.

As pointed out by Ueyama et al. (2020), estimated initial jumps in θ and q from operational radiosonde observations can significantly influence the ABL development, and can vary substantially depending on the height at which it was calculated associated with the estimated ABL height. While lapse rates in the free atmosphere were similar and supported by observations, the same assumption as lapse rates in the model for initial jumps at the entrainment zone could be another cause of error. Similarly, to Ueyama et al. (2020), model simulations resulted in considerable scatter in daily variations of the ABL height and mixed-layer $\Delta\theta$ and Δq, but the climatology and magnitude of seasonal variations were well captured by the model.

2.7 Conclusion

This study showed the importance of accounting for ABL growth feedbacks in order to fully understand surface climate and ABL dynamics differences at the FTE since near-surface observations might differ from ABL conditions. A distinct influence of surface properties on surface climate and ABL dynamics, which changes between seasons at the FTE was shown. The increasing tree cover at the southern margin of the FTE led to warmer and drier conditions in spring, with albedo being the main driver of temperature differences. In summer, a higher surface conductance at the tundra site led to more energy being used to moisten the atmosphere, reducing sensible heat input to the ABL resulting in shallower ABL heights and a regional cooling of air temperatures.

Ongoing vegetation changes at the FTE are not well understood. Trees do not seem to extend outside their range limits, but rather densify in the Inuvialuit Settlement Region near Inuvik. This densification of the canopy could then exacerbate temperature and humidity differences at the FTE. Further research is needed to understand vegetation shifts at the FTE and predict associated changes in surface climatic conditions. The presence of taller and more productive shrubs has been observed in the tundra. However, their influence on the surface energy balance is not well understood and documented.

Using surface flux measurements along with radiosonde observations allowed us to simulate and characterize surface climate and ABL dynamics differences. This study was possible due to the close proximity of the tower sites and the radiosonde observatory. Integrating continuous automated observations of the atmospheric boundary layer to co-located tower-based flux measurements would greatly enhance our ability to predict regional climate changes across the circumpolar Arctic-boreal region and their feedback on the global climate following ongoing vegetation shifts.

This study established a baseline understanding of the latitudinal variation in surface-atmosphere interactions, surface climate and ABL dynamics across the FTE in northwestern Canada. It presents the current state of energy exchange patterns and their impact on surface climate and ABL dynamics, providing valuable insights for future research in the region. This study contributes to the limited body of research on surface-atmosphere interactions across the FTE and can serve as a valuable reference for future comparisons with other regions.

2.8 Supplementary material

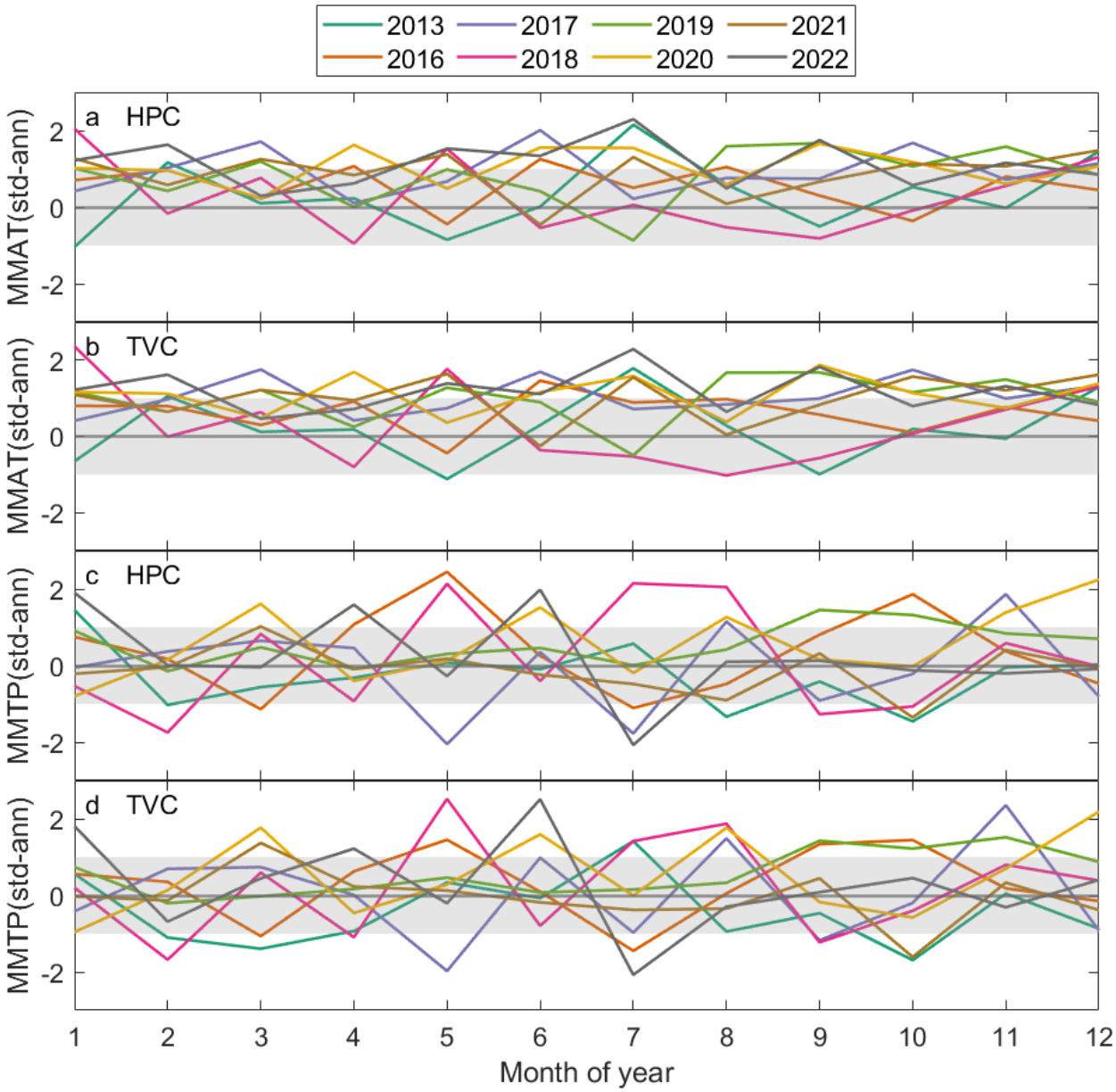

FIGURE S1 - Standardized anomalies (std-ann) of regional mean monthly air temperature (MMAT) for a) the woodland site (HPC) and b) the tundra site (TVC), and of regional mean monthly total precipitation (MMTP) for c) HPC and d) TVC for the period 2013-2022. Shaded areas represent one standard deviation across years. Data source: McKenney et al. (2011).

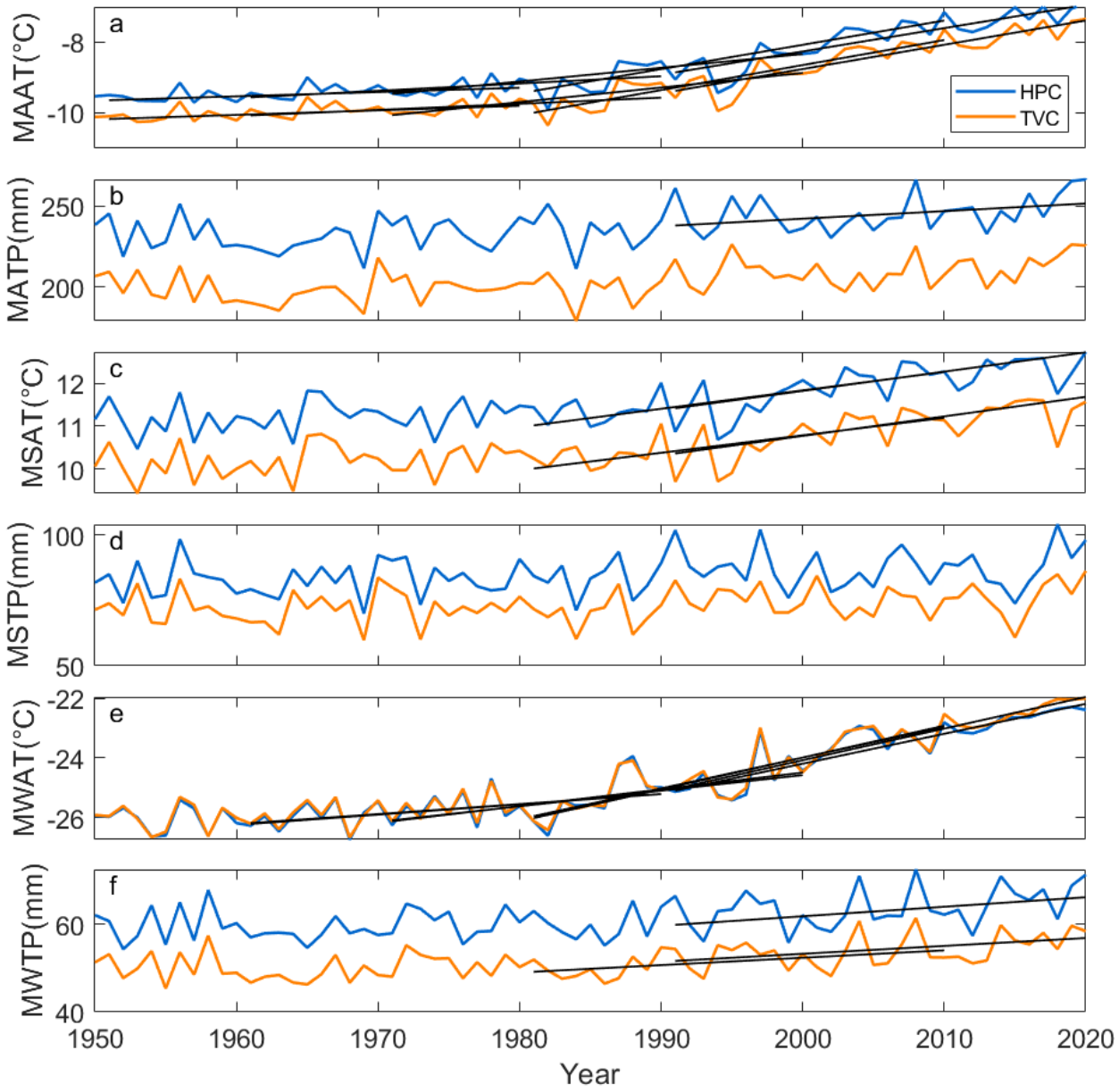

FIGURE S2 - Air temperature and precipitation trends from 1950 to 2020 for the woodland site (HPC, blue) and the tundra site (TVC, orange). Mean annual air temperature (MAAT), mean annual total precipitation (MATP), mean summer air temperature (MSAT), mean summer total precipitation (MSTP), mean winter air temperature (MWAT), mean winter total precipitation (MWTP). Black lines indicate significant increases in the climate normal (30 years period). The significance was tested using the Mann Kendall trend test at a significance level of $\alpha = 0.05$.

To compare differences in atmospheric temperature and humidity profiles between HPC and TVC, we selected campaign-based radiosonde observations on three days that overlapped with days that were used for model simulations. All profiles indicate a higher observed ABL height over HPC than over TVC (**Fig. 2.6**). On August 26th, the ABL height might be underestimated at TVC due to the slightly stable conditions indicated by a slight increase in θ.

The highest ABL height was reached over HPC at around 1700 m on 26 August 2021 and the lowest ABL height was observed over TVC at around 560 m on 13 June 2022. simulated ABL heights for these days were within 150 m from the observed ABL height on 26 August 2021 while observed ABL heights on 8 June 2022 and 13 June 2022 were overestimated by 450 m and 800 m respectively. The mixed layer θ were higher at HPC than at TVC on June 8th and 13th by 0.8°C and 1.7°C, respectively. On August 26th, similar θ were observed. Radiosonde observations at HPC and TVC show similar θ lapse rates in the free atmosphere justifying the use of the same lapse rate for mixed-layer simulations at HPC and TVC.

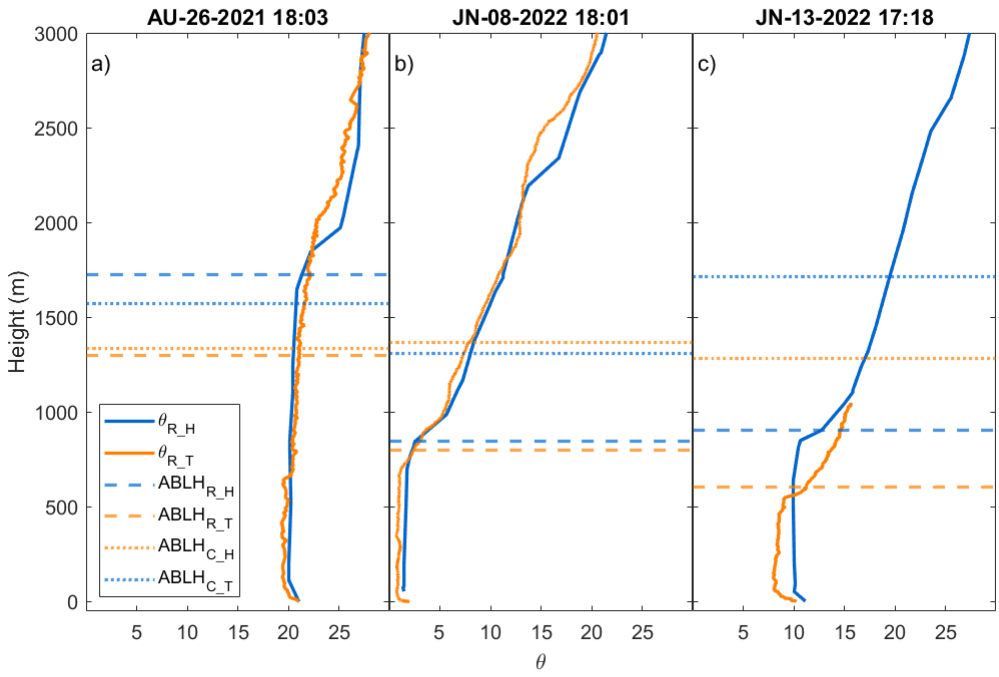

FIGURE S3 - Comparison of potential temperature (θ, °C) profiles at Havikpak Creek (θR_H) and Trail Valley Creek (θR_T) using campaign-based measurements at TVC and operational radiosonde profiles at Inuvik Upper Air Station near Havikpak Creek: observed atmospheric boundary layer height (ABLH, m) at Havikpak Creek (ABLHR_H) and Trail Valley Creek (ABLHR_T) obtained with the 'parcel' method (Holzworth, 1964; Seibert, 2000) and corresponding model estimates obtained with CLASS (ABLHC_H, ABLHC_T).

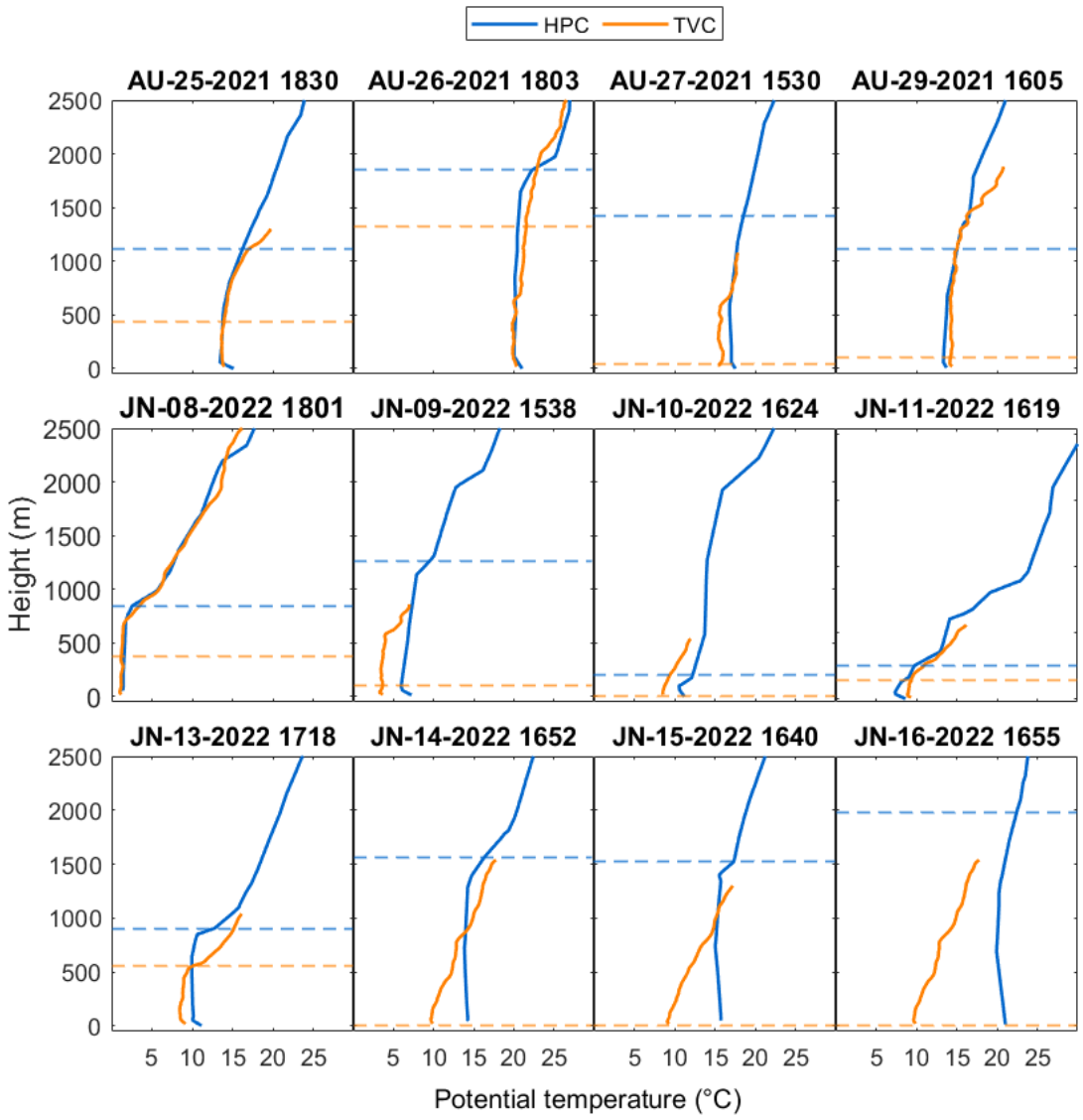

FIGURE S4 - Comparison of vertical potential temperature profiles at HPC and TVC using campaign-based measurements at TVC and operational radiosonde profiles at the Inuvik Upper Air Station around 17:00 MST (UTC - 7h). Dashed lines indicate the observed ABL height according to the parcel method at HPC (blue) and TVC (orange) for the same days.

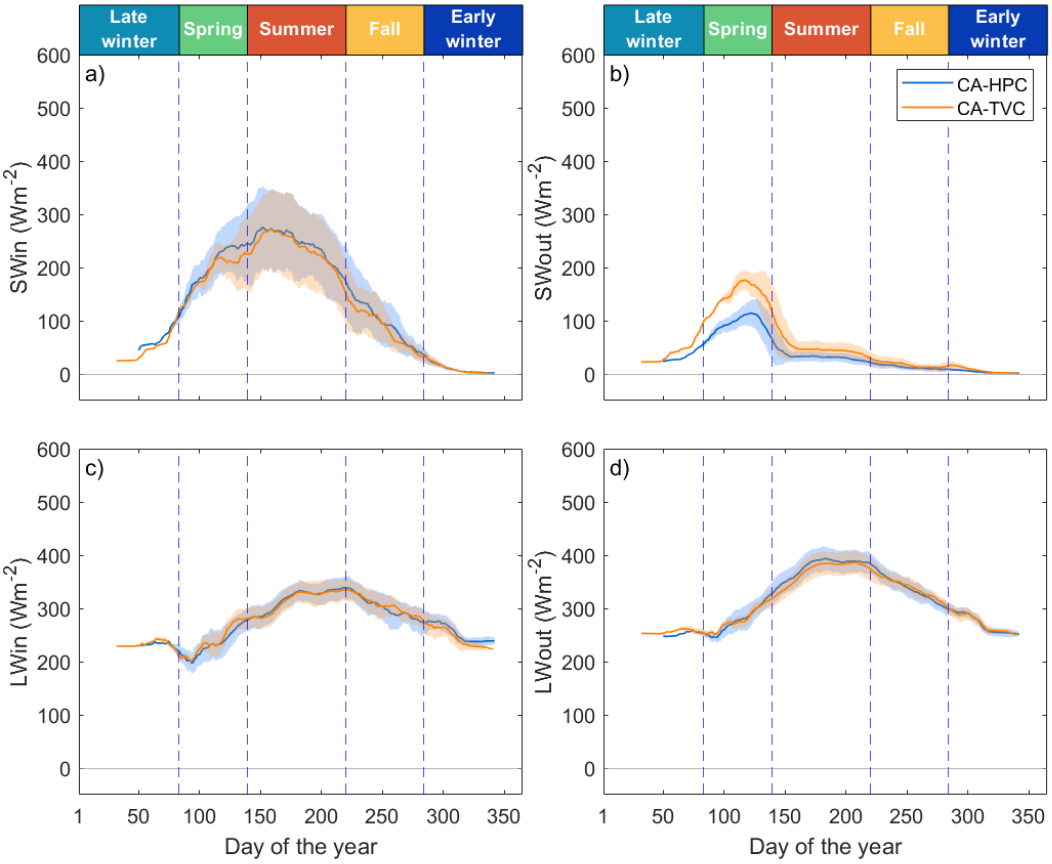

FIGURE S5 - Fourteen-day moving average of daily time series of incoming shortwave radiations (SWin, a), outgoing shortwave radiations (SWout, b), incoming longwave radiations (LWin, c) and outgoing longwave radiations (LWout, d) for the woodland site (HPC) and the tundra site (TVC) across all years (2013-2022). Shaded areas indicate the standard deviation across years.

The modelled seasonal patterns of ABLH, Δθ and Δq at HPC were in good agreement with corresponding radiosonde estimates. CLASS simulations overestimated ABLH by 330 ± 105 m in spring and 130 ± 280 m in summer, while simulations slightly underestimated ABLH in fall by 70 ± 130 m (**Fig S6a)**. Radiosonde estimates of ABLH were characterized by larger interannual variability compared to modelled ABLH. This was particularly the case in summer, when the mean (2013-2022) standard deviation for radiosonde estimates of ABLH was 540 m compared to 280 m for modelled ABLH. A good agreement year-round was found between modelled, and radiosonde estimates of Δθ with differences being smaller than 1 °C in spring, summer and fall (**Fig S6b)**. Modelled decrease in Δq was overestimated in spring and summer by 122 %, 45 % and underestimated by 7 % in fall (**Fig S6c)**. Decreasing Δq over the course of the day suggests that

ABL drying from the entrainment of dry air exceeded moistening from surface water vapour fluxes over the course of a day.

Simulated individual days ABLH, $\Delta\theta$ and Δq showed modest agreement with corresponding radiosonde estimates with R2 below 0.3 for all three variables (**Fig S6d, e, f**). The mean absolute error (MAE) for modelled ABLH of 98 m was close to the mean vertical resolution of the soundings that is around 170 ± 130 m (referring to the distance between radiosonde levels in the first 3,000 m of the afternoon sounding profiles). When radiosonde estimate of $\Delta\theta$ was small, modelled $\Delta\theta$ was overestimated and was underestimated when radiosonde estimate of $\Delta\theta$ was larger than 10°C over the course of a day. The lowest R2 was found for modelled Δq with 0.

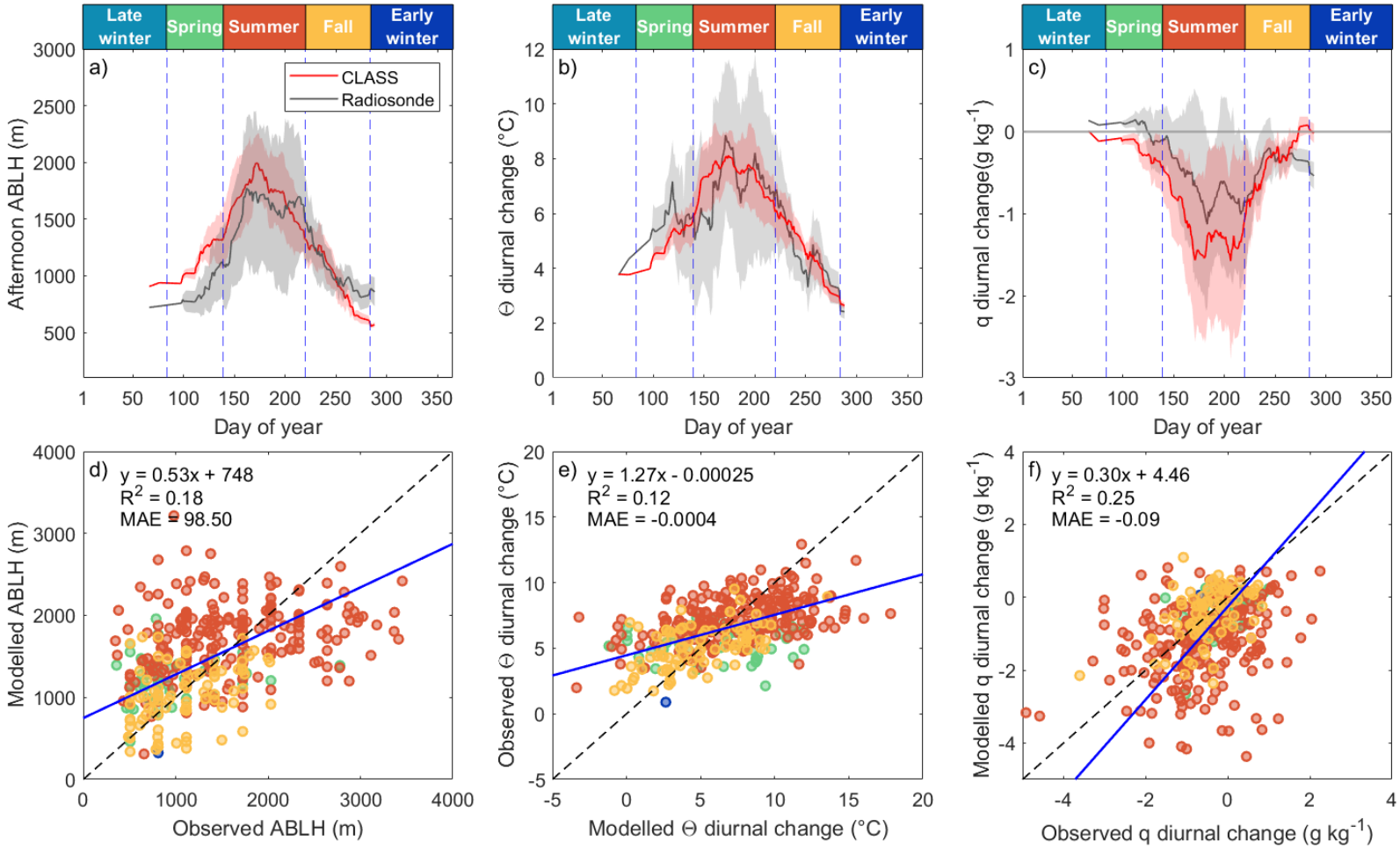

FIGURE S6 - Fourteen-day moving averages in observed (radiosonde) and modelled (CLASS) a) afternoon atmospheric boundary layer height (ABLH), and diurnal changes in b) potential temperature (Δθ) and c) specific humidity (Δq) at Havikpak Creek across all years (2013-2022). Orthogonal linear regression relationships (coefficient of determination [R2], mean average error [MAE]) between modelled and radiosonde estimates of d) ABLH e) Δθ and f) Δq for individual days between 2013 and 2022.

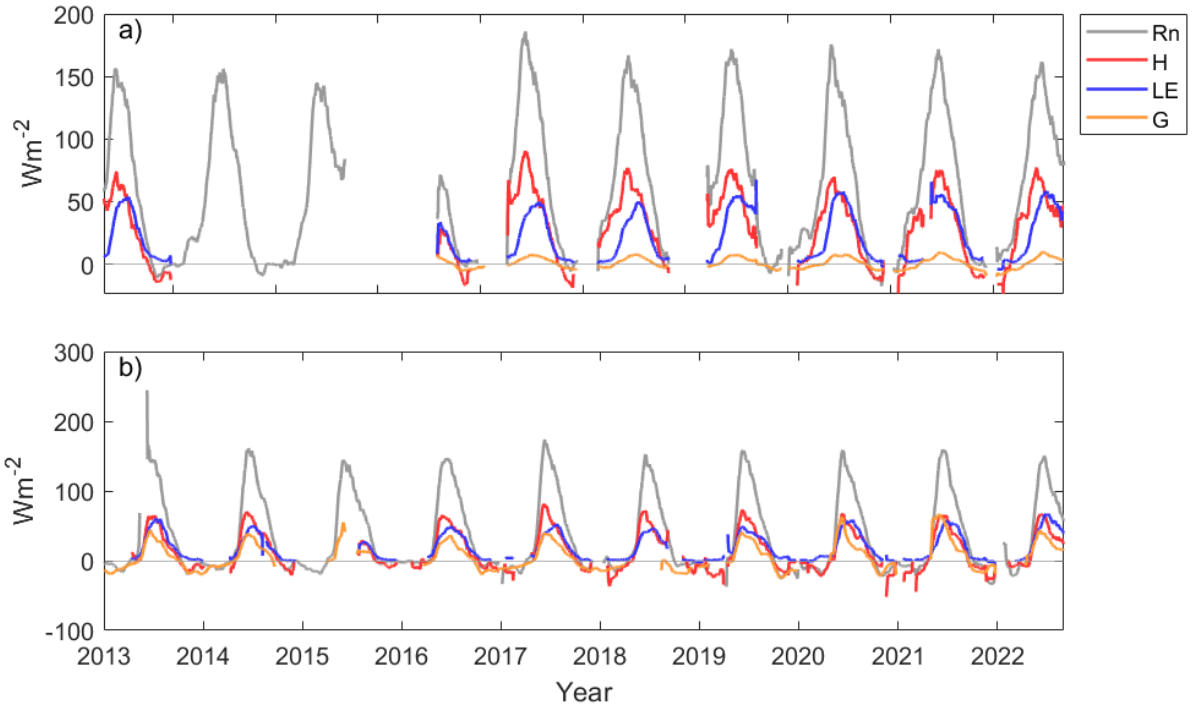

FIGURE S7 - Thirty-day moving average time series of daily net radiations (Rn), sensible heat (H), latent heat (LE) and ground heat fluxes (G) for a) the woodland site (HPC) and b) the tundra site (TVC) across all years (2013-2022).

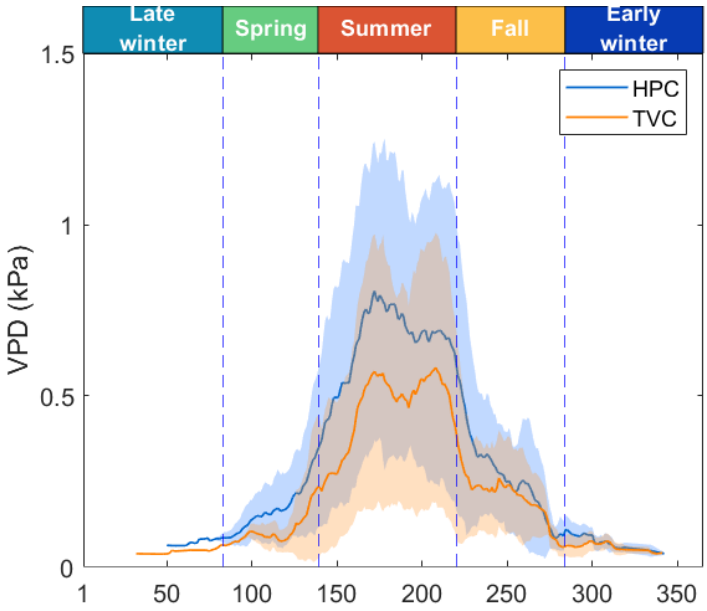

FIGURE S8 - Fourteen-day moving average of seasonal variation in VPD at the woodland site (HPC) and the tundra site (TVC) across all years (2013-2022). Shaded areas indicate the standard deviation.

Conclusion

The goal of this study was to develop a baseline understanding of the latitudinal variation in surface-atmosphere interactions and surface climatic conditions across the forest-tundra ecotone in northwestern Canada. We used paired eddy covariance and supporting environmental measurements to show an increasing dominance of sensible heat exchanges with the atmosphere at a subarctic woodland in comparison to a mineral tundra. A lower Bowen ratio and a higher evaporative fraction showed that more of the available energy was used to moisten the atmosphere at the tundra site than at the woodland. The largest difference occurred in spring, when darker trees masked the snow albedo and much more energy was available at the subarctic woodland. Differences in the surface energy balance shrank in summer and fall, when more and more energy was used at the subarctic woodland to moisten the atmosphere, which could partly explain smaller temperature differences later in the growing season. These differences were interpreted with the help of bulk surface parameters. We showed that the presence of trees at the subarctic woodland led to a stronger influence of larger-scale meteorological parameters, such as VPD, on moisture flux. It also enhances the ability to transfer heat and matter into the atmosphere while increasing the resistance to evapotranspiration.

Using radiosonde observations along with CLASS was necessary to fully understand the role of surface properties on land surface-atmosphere interactions and their influence on surface climatic conditions. The modelling experiment showed important variations in the atmospheric boundary layer height, mixed layer potential air temperature and specific humidity between the subarctic woodland and the tundra depending on the season. While spring differences in potential temperature and specific humidity were mostly explained by the large difference in albedo and available energy, the height of the atmospheric boundary layer played an important role in shaping them in summer.

The larger sensible heat input to the atmosphere at the subarctic woodland, from both surface and entrainment fluxes, led to a higher atmospheric boundary layer, resulting in higher potential temperatures in summer. With a similar latent heat flux at both sites, the atmosphere was cooler at the tundra site where the atmospheric boundary layer was shallower. Differences in modelled potential temperature in the atmospheric boundary layer followed a similar seasonal pattern as differences in atmospheric boundary layer height. The modelling experiment showed a

clear distinction between potential temperature and specific humidity at the surface and within the atmospheric boundary layer. In spring, surface potential temperature differences between the subarctic woodland and the tundra were up to 10°C in the atmospheric boundary layer while reaching 3°C near the surface. This difference emphasizes the need to consider atmospheric boundary layer feedbacks to understand surface climate differences. In spring 70% of modelled diurnal changes in mixed layer potential temperature was attributed to surface sensible heat flux. This contribution slightly decreased to around two thirds in summer and fall. The contribution of entrainment fluxes could partly explain differences between potential temperature at the surface and in the mixed layer.

This study has also demonstrated similarities in land surface-atmosphere interactions with the forest-tundra ecotone at the Seward Peninsula in western Alaska (Beringer et al., 2005). This suggests that similar processes control the partitioning of the energy in our study region.

The results presented here suggest that tree or shrub densification or encroachment at the FTE could potentially increase air temperature and cause high rates of sensible heat exchange and deep atmospheric boundary layer that would enhance the VPD at the FTE (Baldocchi et al., 2000). In the Inuvialuit Settlement Region, an increase in stand and stem density of trees within their range limits and shrub encroachment seems to be occurring (Lantz et al., 2019; Nill et al., 2022; Travers-Smith & Lantz, 2020). This suggests that the density of Subarctic woodlands increasing across the circumarctic and highlights the need for additional research to determine the extent and magnitude of change (Lantz et al., 2019). The increasing drought stress on vegetation could increase the vulnerability to wildfire. Sedano & Randerson (2014) found a significant relationship between VPD and the likelihood that a lightning strike would develop into a fire ignition. In the first week after ignition, above average VPD increased the probability that fires would grow to large or very large sizes. Wildfires frequency is expected to increase at the northern FTE as climate continues to warm (Chen et al., 2021; Young et al., 2017). A change in fire regime at the FTE could shift ecosystems from a carbon sink to a carbon source to the atmosphere and enhance permafrost degradation (Schuur et al., 2008; Walker et al., 2019). Wildfire could also facilitate recruitment of boreal species into areas historically dominated by tundra vegetation (Landhausser & Wein, 1993). Vegetation shifts will also influence regional precipitation patterns and cloud formation, but further research is needed (Vila-Guerau de Arellano et al., 2015).

The field work conducted for this study, which involved the deployment of 40 weather balloons in the arctic tundra, required a significant amount of effort and resources for a relatively small amount of usable data. Integrating continuous, automated observations of the atmospheric boundary layer such as automatic lidars and ceilometers could help to better understand land surface-atmosphere interactions at the FTE. This could also help to reduce the uncertainty related to day-to-day variations that was observed in this study, by providing more continuous observations of daily ABL height variations.

Despite the importance of Arctic-boreal regions on the global climate, our understanding of the drivers of regional climate in these areas remains limited. Careful characterization of regional climates is important as changes in regional climates following ongoing vegetation shifts could feed back on the global system. By examining surface-atmosphere interactions across the forest-tundra ecotone in northwestern Canada, this study adds to this small body of research and provides a valuable point of reference for future comparative studies in other regions.

References

Anderson, R. G., & Wang, D. (2014). Energy budget closure observed in paired Eddy Covariance towers with increased and continuous daily turbulence. *Agricultural and Forest Meteorology, 184*, 204-209. doi:10.1016/j.agrformet.2013.09.012

Baldocchi, D. (2003). Assessing the eddy covariance technique for evaluating carbon dioxide exchange rates of ecosystems: past, present and future. *Global Change Biology, 9*(4), 479-492. doi:10.1046/j.1365-2486.2003.00629.x

Baldocchi, D., Hincks, B. B., & Meyers, T. P. (1988). Measuring Biosphere-Atmosphere Exchanges of Biologically Related Gases with Micrometeorological Methods. *Ecology, 69*(5), 1331-1340. doi:10.2307/1941631

Baldocchi, D., Kelliher, F. M., Black, T. A., & Jarvis, P. (2000). Climate and vegetation controls on boreal zone energy exchange. *Global Change Biology, 6*(S1), 69-83. doi:10.1046/j.1365-2486.2000.06014.x

Baldocchi, D., & Ma, S. (2013). How will land use affect air temperature in the surface boundary layer? Lessons learned from a comparative study on the energy balance of an oak savanna and annual grassland in California, USA. *Tellus B: Chemical and Physical Meteorology, 65*(1). doi:10.3402/tellusb.v65i0.19994

Baltzer, J. L., Day, N. J., Walker, X. J., Greene, D., Mack, M. C., Alexander, H. D., . . . Johnstone, J. F. (2021). Increasing fire and the decline of fire adapted black spruce in the boreal forest. *Proc Natl Acad Sci U S A, 118*(45). doi:10.1073/pnas.2024872118

Beck, H. E., Zimmermann, N. E., McVicar, T. R., Vergopolan, N., Berg, A., & Wood, E. F. (2018). Present and future Koppen-Geiger climate classification maps at 1-km resolution. *Sci Data, 5*, 180214. doi:10.1038/sdata.2018.214

Beringer, J., Chapin, F. S., Thompson, C. C., & McGuire, A. D. (2005). Surface energy exchanges along a tundra-forest transition and feedbacks to climate. *Agricultural and Forest Meteorology, 131*(3-4), 143-161. doi:10.1016/j.agrformet.2005.05.006

Beringer, J., Tapper, N. J., McHugh, I., Chapin, F. S., Lynch, A. H., Serreze, M. C., & Slater, A. (2001). Impact of Arctic treeline on synoptic climate. *GEOPHYSICAL RESEARCH LETTERS, 28*(22), 4247-4250. doi:10.1029/2001gl012914

Berner, L. T., & Goetz, S. J. (2022). Satellite observations document trends consistent with a boreal forest biome shift. *Glob Chang Biol*. doi:10.1111/gcb.16121

Bessardon, G. E. Q., Fosu-Amankwah, K., Petersson, A., & Brooks, B. J. (2019). Evaluation of Windsond S1H2 performance in Kumasi during the 2016 DACCIWA field campaign. *Atmospheric Measurement Techniques, 12*(2), 1311-1324. doi:10.5194/amt-12-1311-2019

Callaghan, T. V., Crawford, R. M. M., Eronen, M., Hofgaard, A., Payette, S., Rees, W. G., . . . Werkman, B. R. (2002). The Dynamics of the Tundra-Taiga Boundary: An Overview and Suggested Coordinated and Integrated Approach to Research. *Ambio*, 3-5. Retrieved from http://www.jstor.org/stable/25094569

Chapin, F. S., Sturm, M., Serreze, M. C., McFadden, J. P., Key, J. R., Lloyd, A. H., . . . Welker, J. M. (2005). Role of land-surface changes in arctic summer warming. *Science, 310*(5748), 657-660. doi:10.1126/science.1117368

Chylek, P., Folland, C., Klett, J. D., Wang, M., Hengartner, N., Lesins, G., & Dubey, M. K. (2022). Annual Mean Arctic Amplification 1970–2020: Observed and Simulated by CMIP6 Climate Models. *GEOPHYSICAL RESEARCH LETTERS, 49*(13). doi:10.1029/2022gl099371

Cifarelli, L., Brunetti, M., Prodi, F., & Wagner, F. (2015). The climate system. *EPJ Web of Conferences, 98*. doi:10.1051/epjconf/20159802001

Denissen, J. M. C., Orth, R., Wouters, H., Miralles, D. G., van Heerwaarden, C. C., de Arellano, J. V.-G., & Teuling, A. J. (2021). Soil moisture signature in global weather balloon soundings. *npj Climate and Atmospheric Science, 4*(1). doi:10.1038/s41612-021-00167-w

Eaton, A. K., Rouse, W. R., Lafleur, P. M., Marsh, P., & Blanken, P. D. (2001). Surface Energy Balance of the Western and Central Canadian Subarctic: Variations in the Energy Balance among Five Major Terrain Types. *Journal of Climate, 14*(17), 3692-3703. doi:10.1175/1520-0442(2001)014<3692:Sebotw>2.0.Co;2

Eugster, W., Rouse, W. R., Pielke Sr, R. A., McFadden, J. P., Baldocchi, D. D., Kittel, T. G. F., . . . Chambers, S. (2000). Land-atmosphere energy exchange in Arctic tundra and boreal forest: available data and feedbacks to climate. *Global Change Biology, 6*(S1), 84-115. doi:10.1046/j.1365-2486.2000.06015.x

Foster, A. C., Wang, J. A., Frost, G. V., Davidson, S. J., Hoy, E., Turner, K. W., . . . Goetz, S. (2022). Disturbances in North American boreal forest and Arctic tundra: impacts, interactions, and responses. *Environmental Research Letters, 17*(11). doi:10.1088/1748-9326/ac98d7

Gibson, C., Cottenie, K., Gingras-Hill, T., Kokelj, S. V., Baltzer, J. L., Chasmer, L., & Turetsky, M. R. (2021). Mapping and understanding the vulnerability of northern peatlands to permafrost thaw at scales relevant to community adaptation planning. *Environmental Research Letters, 16*(5). doi:10.1088/1748-9326/abe74b

Goetz, S. J., Bunn, A. G., Fiske, G. J., & Houghton, R. A. (2005). Satellite-observed photosynthetic trends across boreal North America associated with climate and fire disturbance. *Proc Natl Acad Sci U S A, 102*(38), 13521-13525. doi:10.1073/pnas.0506179102

Gonzalez, P., Neilson, R. P., Lenihan, J. M., & Drapek, R. J. (2010). Global patterns in the vulnerability of ecosystems to vegetation shifts due to climate change. *Global Ecology and Biogeography, 19*(6), 755-768. doi:10.1111/j.1466-8238.2010.00558.x

Gruber, S. (2012). Derivation and analysis of a high-resolution estimate of global permafrost zonation. *The Cryosphere, 6*(1), 221-233. doi:10.5194/tc-6-221-2012

Hansen, M. C., P. V. Potapov, R. Moore, M. Hancher, S. A. Turubanova, A. Tyukavina, D. Thau, S. V. Stehman, S. J. Goetz, T. R. Loveland, A. Kommareddy, A. Egorov, L. Chini, C. O. Justice, and J. R. G. Townshend. 2013. "High-Resolution Global Maps of 21st-Century Forest Cover Change." Science 342 (15 November): 850-53. Data available on-line at: https://glad.earthengine.app/view/global-forest-change.

Harsch, M. A., Hulme, P. E., McGlone, M. S., & Duncan, R. P. (2009). Are treelines advancing? A global meta-analysis of treeline response to climate warming. *Ecol Lett, 12*(10), 1040-1049. doi:10.1111/j.1461-0248.2009.01355.x

Helbig, Pappas, C., & Sonnentag, O. (2016). Permafrost thaw and wildfire: Equally important drivers of boreal tree cover changes in the Taiga Plains, Canada. *GEOPHYSICAL RESEARCH LETTERS, 43*(4), 1598-1606. doi:10.1002/2015gl067193

Helbig, M., Chasmer, L. E., Desai, A. R., Kljun, N., Quinton, W. L., & Sonnentag, O. (2017). Direct and indirect climate change effects on carbon dioxide fluxes in a thawing boreal forest-wetland landscape. *Glob Chang Biol, 23*(8), 3231-3248. doi:10.1111/gcb.13638

Helbig, M., Waddington, J. M., Alekseychik, P., Amiro, B. D., Aurela, M., Barr, A. G., . . . Zyrianov, V. (2020). The biophysical climate mitigation potential of boreal peatlands during the growing season. *Environmental Research Letters*. doi:10.1088/1748-9326/abab34

Helbig., Wischnewski, K., Kljun, N., Chasmer, L. E., Quinton, W. L., Detto, M., & Sonnentag, O. (2016). Regional atmospheric cooling and wetting effect of permafrost thaw-induced boreal forest loss. *Glob Chang Biol, 22*(12), 4048-4066. doi:10.1111/gcb.13348

hen, Y., Romps, D. M., Seeley, J. T., Veraverbeke, S., Riley, W. J., Mekonnen, Z. A., & Randerson, J. T. (2021). Future increases in Arctic lightning and fire risk for permafrost carbon. Nature Climate Change, 11(5), 404-410. doi:10.1038/s41558-021-01011-y

Hersbach, H., Bell, B., Berrisford, P., Biavati, G., Horányi, A., Muñoz Sabater, J., Nicolas, J., Peubey, C., Radu, R., Rozum, I., Schepers, D., Simmons, A., Soci, C., Dee, D., Thépaut, J-N. (2023): ERA5 hourly data on pressure levels from 1940 to present. Copernicus Climate Change Service (C3S) Climate Data Store (CDS), DOI: 10.24381/cds.bd0915c6 (Accessed on 23-04-2023)

Hinzman, L. D., Bettez, N. D., Bolton, W. R., Chapin, F. S., Dyurgerov, M. B., Fastie, C. L., . . . Yoshikawa, K. (2005). Evidence and Implications of Recent Climate Change in Northern Alaska and Other Arctic Regions. *Climatic Change, 72*(3), 251-298. doi:10.1007/s10584-005-5352-2

Holtmeier, F. K., & Broll, G. E. (2007). Treeline advance - driving processes and adverse factors. *Landscape Online, 1*, 1-33. doi:10.3097/lo.200701

Holzworth, G. C. (1964). Estimates of Mean Maximum Mixing Depths in the Contiguous United States. *Monthly Weather Review, 92*(5), 235-242. doi:10.1175/1520-0493(1964)092<0235:Eommmd>2.3.Co;2

Knauer, J., El-Madany, T. S., Zaehle, S., & Migliavacca, M. (2018). Bigleaf-An R package for the calculation of physical and physiological ecosystem properties from eddy covariance data. *PLoS One, 13*(8), e0201114. doi:10.1371/journal.pone.0201114

Krogh, S. A., & Pomeroy, J. W. (2018). Recent changes to the hydrological cycle of an Arctic basin at the tundra–taiga transition. *Hydrology and Earth System Sciences, 22*(7), 3993-4014. doi:10.5194/hess-22-3993-2018

Kukavskaya, E. A., Buryak, L. V., Shvetsov, E. G., Conard, S. G., & Kalenskaya, O. P. (2016). The impact of increasing fire frequency on forest transformations in southern Siberia. *Forest Ecology and Management, 382*, 225-235. doi:10.1016/j.foreco.2016.10.015

Lafleur, P. M., & Rouse, W. R. (1995). Energy partitioning at treeline forest and tundra sites and its sensitivity to climate change. *Atmosphere-Ocean, 33*(1), 121-133. doi:10.1080/07055900.1995.9649527

Landhausser, S. M., & Wein, R. W. (1993). Postfire Vegetation Recovery and Tree Establishment at the Arctic Treeline: Climate-Change-Vegetation-Response Hypotheses. The Journal of Ecology, 81(4). doi:10.2307/2261664

Lantz, T. C., Gergel, S. E., & Kokelj, S. V. (2010). Spatial Heterogeneity in the Shrub Tundra Ecotone in the Mackenzie Delta Region, Northwest Territories: Implications for Arctic Environmental Change. *Ecosystems, 13*(2), 194-204. doi:10.1007/s10021-009-9310-0

Lantz, T. C., Marsh, P., & Kokelj, S. V. (2012). Recent Shrub Proliferation in the Mackenzie Delta Uplands and Microclimatic Implications. *Ecosystems, 16*(1), 47-59. doi:10.1007/s10021-012-9595-2

Lantz, T. C., Moffat, N. D., Fraser, R. H., & Walker, X. (2019). Reproductive limitation mediates the response of white spruce (Picea glauca) to climate warming across the forest–tundra ecotone. *Arctic Science, 5*(4), 167-184. doi:10.1139/as-2018-0012

Lasslop, G., Reichstein, M., Kattge, J., & Papale, D. (2008). Influences of observation errors in eddy flux data on inverse model parameter estimation. *Biogeosciences, 5*(5), 1311-1324. doi:10.5194/bg-5-1311-2008

Lloyd, A. H., & Bunn, A. G. (2007). Responses of the circumpolar boreal forest to 20th century climate variability. *Environmental Research Letters, 2*(4). doi:10.1088/1748-9326/2/4/045013

Lloyd, A. H., Rupp, T. S., Fastie, C. L., & Starfield, A. M. (2002). Patterns and dynamics of treeline advance on the Seward Peninsula, Alaska. *Journal of Geophysical Research, 108*(D2). doi:10.1029/2001jd000852

Marsh, P., & Pomeroy, J. W. (1996). Meltwater Fluxes at an Arctic Forest-Tundra Site. *Hydrological Processes, 10*(10), 1383-1400. doi:10.1002/(sici)1099-1085(199610)10:10<1383::Aid-hyp468>3.0.Co;2-w

Mauder M, Foken T (2011) Documentation and Instruction Manual of the Eddy-Covariance Software Package TK3, pp. 1– 60. Univ. Bayreuth, Abt. Mikrometeorologie, Bayreuth, Germany.

McGuire, A. D., Chapin, F. S., Walsh, J. E., & Wirth, C. (2006). Integrated Regional Changes in Arctic Climate Feedbacks: Implications for the Global Climate System. *Annual Review of Environment and Resources, 31*(1), 61-91. doi:10.1146/annurev.energy.31.020105.100253

McKenney DW, Hutchinson MF, Papadopol P, Lawrence K, Pedlar J, Campbell K, Milewska E, Hopkinson RF, Price D, Owen T (2011): Customized spatial climate models for North America. Bulletin of the American Meteorological Society 92: 1611-1622.

McNaughton, K. G., & Spriggs, T. W. (1986). A mixed-layer model for regional evaporation. *Boundary-Layer Meteorology, 34*(3), 243-262. doi:10.1007/bf00122381

Moncrieff, J. B., Malhi, Y., & Leuning, R. (1996). The propagation of errors in long-term measurements of land-atmosphere fluxes of carbon and water. *Global Change Biology, 2*(3), 231-240. doi:10.1111/j.1365-2486.1996.tb00075.x

Moncrieff, J. B., Massheder, J. M., de Bruin, H., Elbers, J., Friborg, T., Heusinkveld, B., . . . Verhoef, A. (1997). A system to measure surface fluxes of momentum, sensible heat, water vapour and carbon dioxide. *Journal of Hydrology, 188-189*, 589-611. doi:10.1016/s0022-1694(96)03194-0

Monteith, J. L. 1965. Evaporation and environment. Symposia of the Society for Experimental Biology. 19, pp. 205-234.

Myers-Smith, I. H., Forbes, B. C., Wilmking, M., Hallinger, M., Lantz, T., Blok, D., . . . Hik, D. S. (2011). Shrub expansion in tundra ecosystems: dynamics, impacts and research priorities. *Environmental Research Letters, 6*(4). doi:10.1088/1748-9326/6/4/045509

Nill, L., Grünberg, I., Ullmann, T., Gessner, M., Boike, J., & Hostert, P. (2022). Arctic shrub expansion revealed by Landsat-derived multitemporal vegetation cover fractions in the Western Canadian Arctic. *Remote Sensing of Environment, 281*. doi:10.1016/j.rse.2022.113228

Oechel, W. C., Laskowski, C. A., Burba, G., Gioli, B., & Kalhori, A. A. M. (2014). Annual patterns and budget of CO2 flux in an Arctic tussock tundra ecosystem. *Journal of Geophysical Research: Biogeosciences, 119*(3), 323-339. doi:10.1002/2013jg002431

Papale, D., Reichstein, M., Aubinet, M., Canfora, E., Bernhofer, C., Kutsch, W., . . . Yakir, D. (2006). Towards a standardized processing of Net Ecosystem Exchange measured with eddy covariance technique: algorithms and uncertainty estimation. *Biogeosciences, 3*(4), 571-583. doi:10.5194/bg-3-571-2006

Pearson, R. G., Phillips, S. J., Loranty, M. M., Beck, P. S. A., Damoulas, T., Knight, S. J., & Goetz, S. J. (2013). Shifts in Arctic vegetation and associated feedbacks under climate change. *Nature Climate Change, 3*(7), 673-677. doi:10.1038/nclimate1858

Phoenix, G. K., & Bjerke, J. W. (2016). Arctic browning: extreme events and trends reversing arctic greening. *Glob Chang Biol, 22*(9), 2960-2962. doi:10.1111/gcb.13261

R Core Team (2020). R: A language and environment for statistical computing. R Foundation for Statistical Computing, Vienna, Austria. URL https://www.R-project.org/

Rantanen, M., Karpechko, A. Y., Lipponen, A., Nordling, K., Hyvärinen, O., Ruosteenoja, K., . . . Laaksonen, A. (2022). The Arctic has warmed nearly four times faster than the globe since 1979. *Communications Earth & Environment, 3*(1). doi:10.1038/s43247-022-00498-3

Rees, W. G., Hofgaard, A., Boudreau, S., Cairns, D. M., Harper, K., Mamet, S., . . . Tutubalina, O. (2020). Is subarctic forest advance able to keep pace with climate change? *Glob Chang Biol, 26*(7), 3965-3977. doi:10.1111/gcb.15113

Reichstein, M., Falge, E., Baldocchi, D., Papale, D., Aubinet, M., Berbigier, P., . . . Valentini, R. (2005). On the separation of net ecosystem exchange into assimilation and ecosystem respiration: review and improved algorithm. *Global Change Biology, 11*(9), 1424-1439. doi:10.1111/j.1365-2486.2005.001002.x

Rey-Sanchez, C., Wharton, S., Vilà-Guerau de Arellano, J., Paw U, K. T., Hemes, K. S., Fuentes, J. D., . . . Baldocchi, D. (2021). Evaluation of Atmospheric Boundary Layer Height From Wind Profiling Radar and Slab Models and Its Responses to Seasonality of Land Cover, Subsidence, and Advection. *Journal of Geophysical Research: Atmospheres, 126*(7). doi:10.1029/2020jd033775

Ryu, Y., Baldocchi, D. D., Ma, S., & Hehn, T. (2008). Interannual variability of evapotranspiration and energy exchange over an annual grassland in California. *Journal of Geophysical Research, 113*(D9). doi:10.1029/2007jd009263

Ryu, Y., Nilson, T., Kobayashi, H., Sonnentag, O., Law, B. E., & Baldocchi, D. D. (2010). On the correct estimation of effective leaf area index: Does it reveal information on clumping effects? *Agricultural and Forest Meteorology, 150*(3), 463-472. doi:10.1016/j.agrformet.2010.01.009

Scheffer, M., Hirota, M., Holmgren, M., Van Nes, E. H., & Chapin, F. S., 3rd. (2012). Thresholds for boreal biome transitions. *Proc Natl Acad Sci U S A, 109*(52), 21384-21389. doi:10.1073/pnas.1219844110

Schuur, E. A. G., Bockheim, J., Canadell, J. G., Euskirchen, E., Field, C. B., Goryachkin, S. V., . . . Zimov, S. A. (2008). Vulnerability of Permafrost Carbon to Climate Change: Implications for the Global Carbon Cycle. BioScience, 58(8), 701-714. doi:10.1641/b580807

Sedano, F., & Randerson, J. T. (2014). Multi-scale influence of vapour pressure deficit on fire ignition and spread in boreal forest ecosystems. *Biogeosciences, 11*(14), 3739-3755. doi:10.5194/bg-11-3739-2014

Seibert, P. (2000). Review and intercomparison of operational methods for the determination of the mixing height. *Atmospheric Environment, 34*(7), 1001-1027. doi:10.1016/s1352-2310(99)00349-0

Seidel, D. J., Ao, C. O., & Li, K. (2010). Estimating climatological planetary boundary layer heights from radiosonde observations: Comparison of methods and uncertainty analysis. *Journal of Geophysical Research, 115*(D16). doi:10.1029/2009jd013680

Sonnentag, O., Chen, J. M., Roberts, D. A., Talbot, J., Halligan, K. Q., & Govind, A. (2007). Mapping tree and shrub leaf area indices in an ombrotrophic peatland through multiple endmember spectral unmixing. *Remote Sensing of Environment, 109*(3), 342-360. doi:10.1016/j.rse.2007.01.010

Sonnentag, O., Talbot, J., Chen, J. M., & Roulet, N. T. (2007). Using direct and indirect measurements of leaf area index to characterize the shrub canopy in an ombrotrophic peatland. *Agricultural and Forest Meteorology, 144*(3-4), 200-212. doi:10.1016/j.agrformet.2007.03.001

Stephens, G. L., O'Brien, D., Webster, P. J., Pilewski, P., Kato, S., & Li, J.-l. (2015). The albedo of Earth. *Reviews of Geophysics, 53*(1), 141-163. doi:10.1002/2014rg000449

Stralberg, D., Wang, X., Parisien, M.-A., Robinne, F.-N., Sólymos, P., Mahon, C. L., . . . Bayne, E. M. (2018). Wildfire-mediated vegetation change in boreal forests of Alberta, Canada. *Ecosphere, 9*(3). doi:10.1002/ecs2.2156

Stull, R. (1988). The Atmospheric Boundary Layer. In A. S. Library (Ed.), *An Introduction to Boundary Layer Meteorology* (Vol. 13): Springer, Dordrecht.

Tape, K. E. N., Sturm, M., & Racine, C. (2006). The evidence for shrub expansion in Northern Alaska and the Pan-Arctic. *Global Change Biology, 12*(4), 686-702. doi:10.1111/j.1365-2486.2006.01128.x

Tennekes, H. (1973). A Model for the Dynamics of the Inversion Above a Convective Boundary Layer. *Journal of the Atmospheric Sciences, 30*(4), 558-567. doi:10.1175/1520-0469(1973)030<0558:Amftdo>2.0.Co;2

Tennekes, H., & Driedonks, A. G. M. (1981). Basic entrainment equations for the atmospheric boundary layer. *Boundary-Layer Meteorology, 20*(4), 515-531. doi:10.1007/bf00122299

Teskey, R. O., Hinckley, T. M., & Grier, C. C. (1984). Temperature-Induced Change in the Water Relations of Abies amabilis (Dougl.) Forbes. *Plant Physiology, 74*(1), 77-80. Retrieved from http://www.jstor.org/stable/4268411

The MathWorks Inc. (2020). MATLAB version: 9.9.0 (R2020b), Natick, Massachusetts: The MathWorks Inc. https://www.mathworks.com

Thom, A. S. (1972). Momentum, mass and heat exchange of vegetation. *Quarterly Journal of the Royal Meteorological Society, 98*(415), 124-134. doi:10.1002/qj.49709841510

Thompson, C., Beringer, J., Chapin, F. S., & McGuire, A. D. (2004). Structural complexity and land-surface energy exchange along a gradient from arctic tundra to boreal forest. *Journal of Vegetation Science, 15*(3), 397-406. doi:10.1111/j.1654-1103.2004.tb02277.x

Timoney, K. P. (2022). Letter to the editor on "Satellite observations document trends consistent with a boreal biome shift". *Glob Chang Biol, 28*(18), 5335-5336. doi:10.1111/gcb.16327

Timoney, K. P., & Mamet, S. (2020). No treeline advance over the last 50 years in subarctic western and central Canada and the problem of vegetation misclassification in remotely sensed data. *Écoscience, 27*(2), 93-106. doi:10.1080/11956860.2019.1698258

Timoney., La Roi, G. H., Zoltai, S. C., & Robinson, A. L. (1992). The High Subarctic Forest-Tundra of Northwestern Canada: Position, Width, and Vegetation Gradients in Relation to Climate. *Arctic, 45*(1). doi:10.14430/arctic1367

Travers-Smith, H. Z., & Lantz, T. C. (2020). Leading-edge disequilibrium in alder and spruce populations across the forest–tundra ecotone. *Ecosphere, 11*(7). doi:10.1002/ecs2.3118

Trenberth, K. E., Fasullo, J. T., & Kiehl, J. (2009). Earth's Global Energy Budget. *Bulletin of the American Meteorological Society, 90*(3), 311-324. doi:10.1175/2008bams2634.1

Ueyama, M., Yamamori, T., Iwata, H., & Harazono, Y. (2020). Cooling and Moistening of the Planetary Boundary Layer in Interior Alaska Due to a Postfire Change in Surface Energy Exchange. *Journal of Geophysical Research: Atmospheres, 125*(18). doi:10.1029/2020jd032968

Van Dijk, A., Moene, A.F., and De Bruin, H.A.R., 2004: The principles of surface flux physics: theory, practice and description of the ECPACK library, Internal Report 2004/1, Meteorology and Air Quality Group, Wageningen University, Wageningen, the Netherlands, 99 pp.

van Heerwaarden, C. C., & Teuling, A. J. (2014). Disentangling the response of forest and grassland energy exchange to heatwaves under idealized land–atmosphere coupling. *Biogeosciences, 11*(21), 6159-6171. doi:10.5194/bg-11-6159-2014

van Heerwaarden, C. C., Vilà-Guerau de Arellano, J., Moene, A. F., & Holtslag, A. A. M. (2009). Interactions between dry-air entrainment, surface evaporation and convective boundary-layer development. *Quarterly Journal of the Royal Meteorological Society, 135*(642), 1277-1291. doi:10.1002/qj.431

Vickers, D., & Mahrt, L. (1997). Quality Control and Flux Sampling Problems for Tower and Aircraft Data. *Journal of Atmospheric and Oceanic Technology, 14*(3), 512-526. doi:10.1175/1520-0426(1997)014<0512:Qcafsp>2.0.Co;2

Vila-Guerau de Arellano, J., C. van Heerwaarden, C., J. H. van Stratum, B., & van den Dries, K. (2015). *Atmospheric Boundary Layer*.

Vila-Guerau de Arellano, J., Gioli, B., Miglietta, F., Jonker, H. J. J., Klein Baltink, H., Hutjes, R. W. A., & Holtslag, A. A. M. (2004). Entrainment process of carbon dioxide in the atmospheric boundary layer. *Journal of Geophysical Research, 109*(D18). doi:10.1029/2004jd004725

Walker, X. J., Baltzer, J. L., Cumming, S. G., Day, N. J., Ebert, C., Goetz, S., . . . Mack, M. C. (2019). Increasing wildfires threaten historic carbon sink of boreal forest soils. Nature, 572(7770), 520-523. doi:10.1038/s41586-019-1474-y

Walker, X. J., Rogers, B. M., Veraverbeke, S., Johnstone, J. F., Baltzer, J. L., Barrett, K., . . . Mack, M. C. (2020). Fuel availability not fire weather controls boreal wildfire severity and carbon emissions. *Nature Climate Change, 10*(12), 1130-1136. doi:10.1038/s41558-020-00920-8

Wallace, C. A., & Baltzer, J. L. (2019). Tall Shrubs Mediate Abiotic Conditions and Plant Communities at the Taiga–Tundra Ecotone. *Ecosystems, 23*(4), 828-841. doi:10.1007/s10021-019-00435-0

Wang, J. A., Sulla-Menashe, D., Woodcock, C. E., Sonnentag, O., Keeling, R. F., & Friedl, M. A. (2020). Extensive land cover change across Arctic-Boreal Northwestern North America from disturbance and climate forcing. *Glob Chang Biol, 26*(2), 807-822. doi:10.1111/gcb.14804

Webb, E. K., Pearman, G. I., & Leuning, R. (1980). Correction of flux measurements for density effects due to heat and water vapour transfer. *Quarterly Journal of the Royal Meteorological Society, 106*(447), 85-100. doi:10.1002/qj.49710644707

Wilcox, E. J., Keim, D., de Jong, T., Walker, B., Sonnentag, O., Sniderhan, A. E., . . . Marsh, P. (2019). Tundra shrub expansion may amplify permafrost thaw by advancing snowmelt timing. *Arctic Science, 5*(4), 202-217. doi:10.1139/as-2018-0028

Wilczak, J. M., Oncley, S. P., & Stage, S. A. (2001). Sonic Anemometer Tilt Correction Algorithms. *Boundary-Layer Meteorology, 99*(1), 127-150. doi:10.1023/a:1018966204465

Young, A. M., Higuera, P. E., Duffy, P. A., & Hu, F. S. (2017). Climatic thresholds shape northern high-latitude fire regimes and imply vulnerability to future climate change. Ecography, 40(5), 606-617. doi:10.1111/ecog.02205

Zhang, W., Miller, P. A., Smith, B., Wania, R., Koenigk, T., & Döscher, R. (2013). Tundra shrubification and tree-line advance amplify arctic climate warming: results from an individual-based dynamic vegetation model. *Environmental Research Letters, 8*(3). doi:10.1088/1748-9326/8/3/034023

Zhu, Z., Piao, S., Lian, X., Myneni, R. B., Peng, S., & Yang, H. (2017). Attribution of seasonal leaf area index trends in the northern latitudes with "optimally" integrated ecosystem models. *Glob Chang Biol, 23*(11), 4798-4813. doi:10.1111/gcb.13723